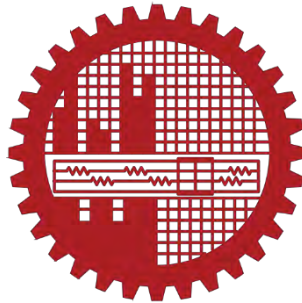# Design and Performance Analysis of Organic Solar Cell

Incorporating Photon Upconverter and Nanoplasmonic Structures

A thesis submitted to the

Department of Electrical and Electronic Engineering (EEE)

of

Bangladesh University of Engineering and Technology (BUET)

In partial fulfillment of the requirement for the degree of

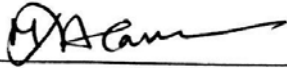MASTER OF SCIENCE IN ELECTRICAL AND ELECTRONIC ENGINEERING

by

Faysal Hakim

(Student ID: 0416062232F)

DEPARTMENT OF ELECTRICAL AND ELECTRONIC ENGINEERING (EEE)

BANGLADESH UNIVERSITY OF ENGINEERING AND TECHNOLOGY (BUET)

November 2018

i

The thesis titled '**Design and Performance Analysis of Organic Solar Cell Incorporating Photon Upconverter and Nanoplasmonic Structures**' submitted by Faysal Hakim, Roll No.: 0416062232 F, Session: April 2016, has been accepted as satisfactory in partial fulfillment of the requirement for the degree of MASTER OF SCIENCE IN ELECTRICAL AND ELECTRONIC ENGINEERING on November 10, 2018.

<u>**Board of Examiners**</u>

1. **Dr. Md. Kawsar Alam**   (Chairman)
   Associate Professor   (Supervisor)
   Department of Electrical and Electronic Engineering
   Bangladesh University of Engineering and Technology
   Dhaka – 1205.

2. **Dr. Md. Shafiqul Islam**   (Member)
   Professor and Head   (Ex-Officio)
   Department of Electrical and Electronic Engineering
   Bangladesh University of Engineering and Technology
   Dhaka – 1205.

3. **Dr. Md. Ziaur Rahman Khan**   (Member)
   Professor
   Department of Electrical and Electronic Engineering
   Bangladesh University of Engineering and Technology
   Dhaka – 1205.

4. **Dr. Md. Anwarul Abedin**   (Member)
   Professor   (External)
   Department of Electrical and Electronic Engineering
   Dhaka University of Engineering and Technology
   Gazipur – 1700.

ii

Declaration

It is hereby declared that this thesis or any part of it has not been submitted elsewhere for the award of any degree or diploma.

Signature of the candidate

_____

Faysal Hakim

(Roll No.: 0416062232F)

Dedication

To my parents and late maternal grandfather.

Acknowledgements

Abstract

Photovoltaic technology is the most promising alternative to ever exhausting energy resources. However, this form of energy is expensive because of the cost and processing associated with commercialization. In this regard, organic solar cell can be effective since the processing of this kind is cheaper and easier. Nevertheless, organic solar cell research still requires much attention to reach the performance level of inorganic solar cells. In this thesis, we propose a detailed FDTD model to describe upconversion in organic solar cells (OSC) and analyze upconversion process for P3HT:PCBM, PSBTBT:PCBM, PBDTTT-C:PCBM and PTB7-Th:PCBM based OSCs, having different power conversion efficiency (PCE) ranges. For each OSC, our model predicts significant improvement in PCEs when an optimized upconverting layer is attached at the back end of the solar cell. For the most efficient active material PTB7-Th:PCBM, a maximum 17% enhancement in PCE has been recorded. In a separate study, we propose a design of metallic nanowire incorporated PTB7-Th:PCBM solar cell and show that up to 13% enhancement in PCE is possible by introducing plasmonic effect at two distinct wavelengths. Then, we analyze the combined effect of plasmonic resonance and upconverting layer in PTB7-Th:PCBM solar cell and estimate a mere 5% enhancement from individual effect. Finally, we discuss the possibility of stretching the PCEs of upconverting OSCs by utilizing concentrated sun light illumination. At 10 sun illumination, it is possible to enhance PCE beyond 50%. The model developed and results obtained from the study have important implications in current OSC research.

Table of Contents

List of Figures

List of Tables

Chapter 1

Introduction

'Affordable and Clean Energy' has been declared by the United nations (UN) as one of the seventeen (17) sustainable development goals for twenty first century [1]. This is mainly because energy is pivotal in almost all the challenges and opportunities the earth faces. However, the production of energy is directly interlinked with climate change and other environmental issues. Moreover, the conventional sources of energy are being exhausted due to excessive use day by day. Therefore, it is important that the production of energy is clean and easily affordable.

Currently the worlds power consumption is nearly 10 terawatts (TW) which is expected to exceed 30 TW by the year 2050 [2]. To meet the insatiable appetite for energy, the search for 'affordable and clean energy' continues. With ever increasing demand and exhaustion of available resources, solar cell technology has originated as a renewable energy source for its capability and long-term sustainability. Solar or photovoltaic (PV) cells are the cleanest possible energy resources available to earth which converts energy absorbed from sunlight into usable electrical energy. Since, the sun radiates enormous amount of power (nearly 120,000 TW) which is directly available to earth, a PV cell with power conversion efficiency (PCE) of 10% and covering 0.16% of earths' surface would be able to provide 20 TW power alone [3]. Add to that, the energy produced in this way, has virtually no effect on the climate change. However, the cost associated with electrical energy production from PV cells is nearly five times more expensive than that produced from fossil fuels

[4]. So, extensive research is needed to bring down the manufacturing and installation cost of PV cells and solar panels.

1.1 Solar Cell

Solar cell is an electronic device in which a material, commonly known as an active material, absorbs power from sun light and converts them into electricity by a mechanism called photovoltaic effect. The first solar cell was produced in 1946 when Russel Ohl used silicon as an active material [5]. Solar cell research flourished in the year 1970 when the oil prices increased manifold. Starting from 1970, solar cell technology has gone through many various adjustments and upgradation from both fabrication and installation perspective. Solar cells can be broadly classified into three major categories based on their primary active materials. They are as follows: silicon (1st generation) solar cells, semiconductor based (2nd generation) solar cells and novel material based (3rd generation) solar cells. They can be sun-categorized into other types as depicted in figure 1. Figure 2 shows the efficiency trends of various solar cells recorded over the past 50 years.
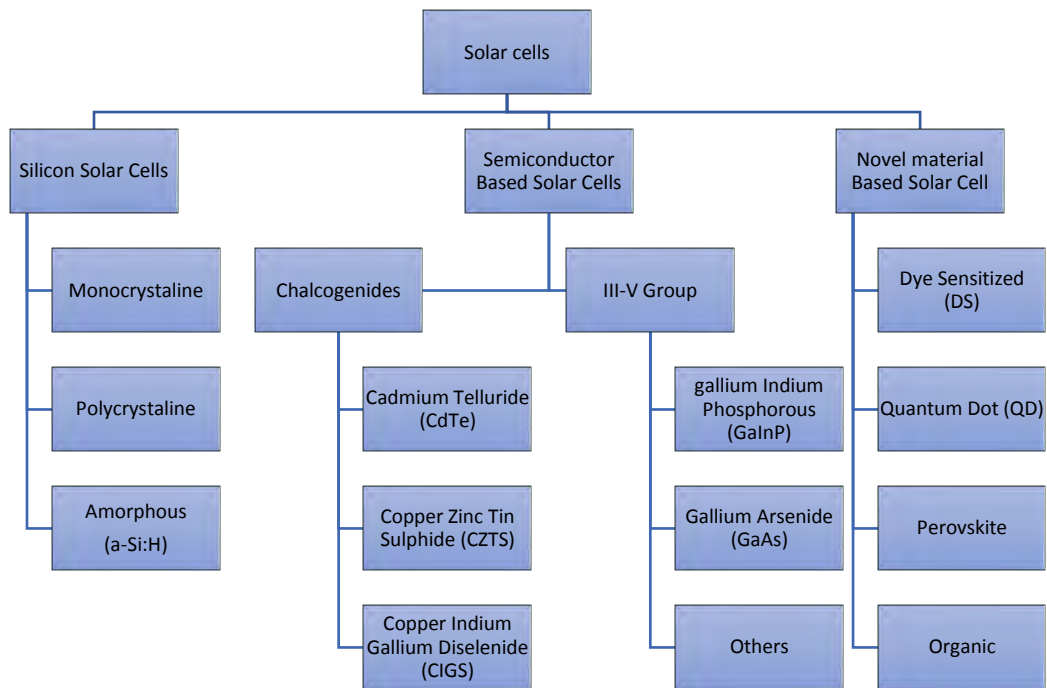
Figure 1: Classification of solar cells based on primary active materials [6]
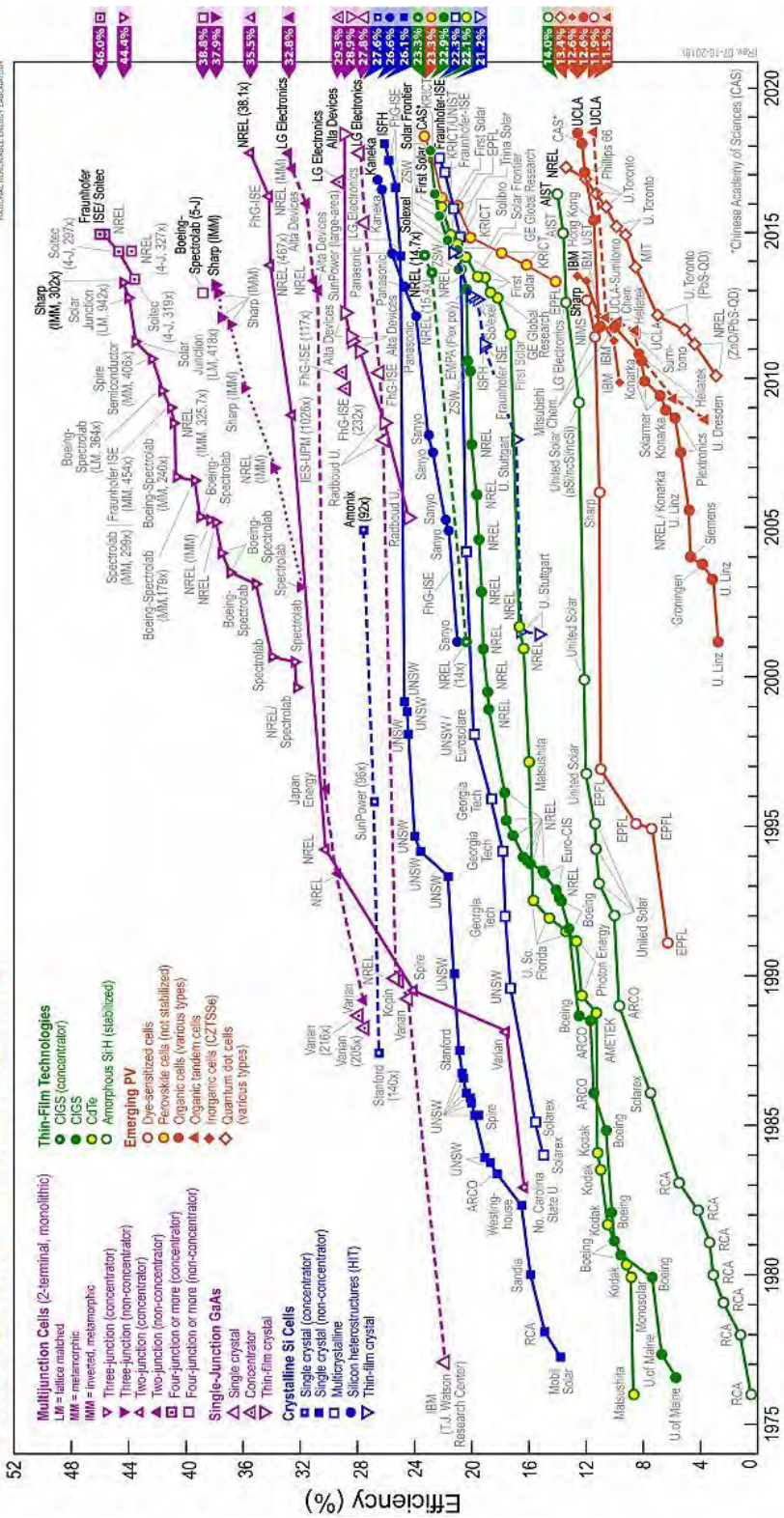
Figure 2: Solar cell efficiency chart [7]

4

1.2 Physics of Solar Cells: Structure and Operation

In the simplest possible structure of a solar cell, the active material (P-N junction) is sandwiched between two electrodes (Figure 3). The active material absorbs energy from sunlight incident on the material. If the energy of the absorbed wavelength (of sunlight) is greater than the bandgap of the active material, electrons in the active material move from valence band to conduction band by absorbing the optical energy and free carriers are generated. The generated free carriers travel to the electrodes by drift (motion due to existing electric field in P-N junction) and diffusion (motion due to concentration gradient) mechanism. Upon reaching the electrodes, the free carriers contribute to current flow in the external circuit connected between electrodes. Thus, electrical power is obtained if a load is attached in between the terminals of two electrodes. During their motion towards the electrodes, some carriers recombine with opposite carries and do not contribute in energy conversion. In short, the basic operation of a solar cell can be divided into:

1. Generation of free carriers
2. Transportation of free carriers towards respective electrodes
3. Collection of free carriers in the electrodes
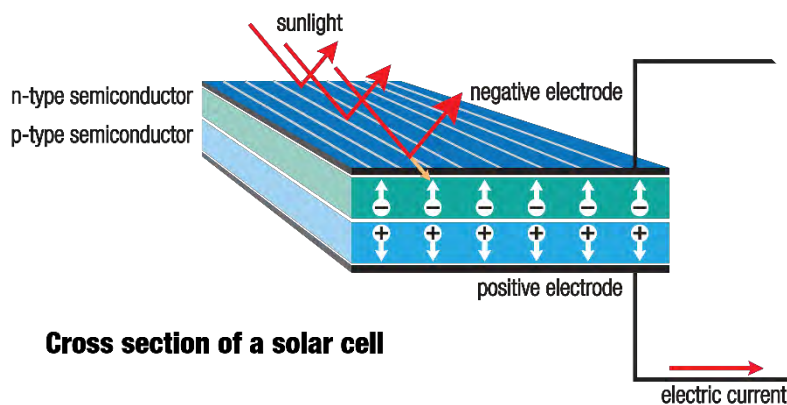
Figure 3: Structure of a simple solar cell

1.3 Characterization of a Solar Cell

The performance of a solar cell is measured in terms of power conversion efficiency (PCE) i.e. the ability of a solar cell to convert optical energy in to electrical energy. The efficiency of a solar cell is defined as the fraction of optical power converted to electrical power.

$$\eta = \frac{P_{out}}{P_{in}} \qquad (1.1)$$

The PCE is estimated from current voltage characteristics of the solar cell. The current-voltage characteristics are often represented graphically, called solar cell I-V or J-V characteristics. Figure 4 shows a solar cell J-V characteristic under illuminated condition.
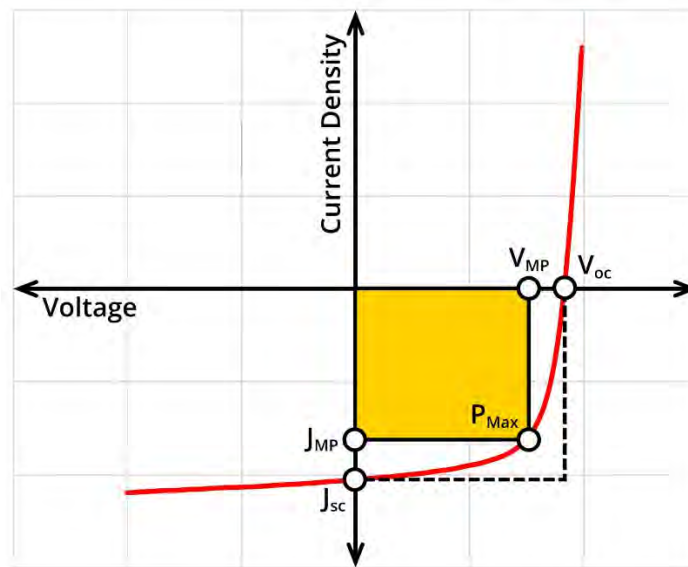
Figure 4: Solar cell J-V characteristics (Colored region and P_{MAX} point denote maximum power)

There are four (4) parameters used to evaluate the performance of a solar cell. They are:

1. Power Conversion Efficiency (η)
2. Short circuit current density (J_{SC})

3. Open circuit Voltage (V_{OC})

4. Fill Factor (FF)

The four parameters are often termed together as figure of merits (FOM) of a solar cell. The short circuit current density is the current through the solar cell per unit cell area when the electrodes are shorted together and thus the voltage across the solar cell is zero. This is the maximum current density that can be obtained from a solar cell. The ideal short circuit current density is the current density obtained from the solar cell when no carriers are lost from the cell due to recombination and other optical and electrical effects. Open circuit voltage, on the other hand, is the maximum voltage that can be achieved from the solar cell. The open circuit voltage is obtained when the terminals are kept open. Here, the free carriers are prevented from leaving the solar cell. So, the carriers accumulate inside the solar cell and create an electric field in opposite direction to the existing electric field in the PN junction. At this condition, the net current is zero. The open circuit voltage increases with increasing bandgap whereas the short circuit current density decreases with increasing bandgap. It is understandable that, at both shorted and open conditions, the power obtained from the solar cell is zero. In fact, the maximum power (P_{MAX}) is obtained at a voltage lower than the open circuit voltage. It is obvious that, at maximum power point, the current density is also lower than the short circuit current density. Fill factor is the ratio between the maximum power and the product of short circuit current and open circuit voltage. The fill factor measures the squareness of a solar cell J-V characteristics.

$$FF = \frac{V_{mp}J_{mp}}{V_{oc}J_{sc}} \tag{1.2}$$

The maximum power, which is also the output power, then can be expressed as,

7

$$P_{max} = V_{oc}J_{sc}FF \qquad (1.3)$$

1.4 Organic Solar Cell

Organic solar cells (OSCs) could be a promising alternative of conventional solar cells due to the abundance of raw materials, its flexibility and thin film architectures [8] - [12]. OSCs can be made 1000 times thinner than silicon solar cells, thereby offering huge savings on materials [13] as well as their processing methods are another major selling point. Both first- and second-generation solar cells depend on vacuum deposition methods requiring massive amount of energy. With polymer based OSCs, on the other hand, layers may be processed from solution and complete solution processed cells are a possibility [14]. In addition, printable solar cell is also a promising aspect of organic materials. However, compared to its inorganic counterpart, the PCE of OSCs are still low (Figure 2). Therefore, optimizing their designs may lead to overall improved efficiency and could reduce the cost of solar energy. The efficiency difference with conventional solar cells shows that there is a huge scope of improvement in OSCs which may be accomplished by engineering the optical and electrical properties of the active materials and other associated layers [15] - [18]. To improve the PCE, the physics of OSCs' must be carefully inspected. Because, the charge generation and transportation mechanism in organic materials are different from that of inorganic materials.

1.4.1 Light Absorption and Carrier Generation

Upon light absorption, OSCs' produce a tightly coupled electron hole pair, called exciton. The low dielectric constant and spatial confinement create strong coulombic attraction in the exciton with binding energy 0.01-1 eV [19]. To separate excitons into free carriers, a donor-acceptor (D/A) architecture is used otherwise the power conversion efficiency would be very low [20]. The donor

8

material has low ionization potential whereas the acceptor material has high electron affinity. At first, the photon is absorbed by the donor material and then exciton is created. When the excitons reach the donor-acceptor interface, the electron is transferred to a material with larger electron affinity and the hole is transferred to a material with lower ionization potential. The electron-hole pair at this stage is called geminate electron hole pair (GEHP). It is understandable that, the interface is the key for exciton separation and thus generation of free carriers. Due to low exciton diffusion lengths (usually ~10 nm) in organic materials, the donor and acceptor materials are mixed together to form an interpenetrating network, called bulk heterojunction (BHJ) [21], [22]. This results in a greater photocurrent, since in BHJ architecture, the interface area increases manifold compared to that of tandem or planar architecture, where donor and acceptor materials are stacked on top of one another [23].

(a)　　　　　　　　　　　(b)　　　　　　　　　　　(c)
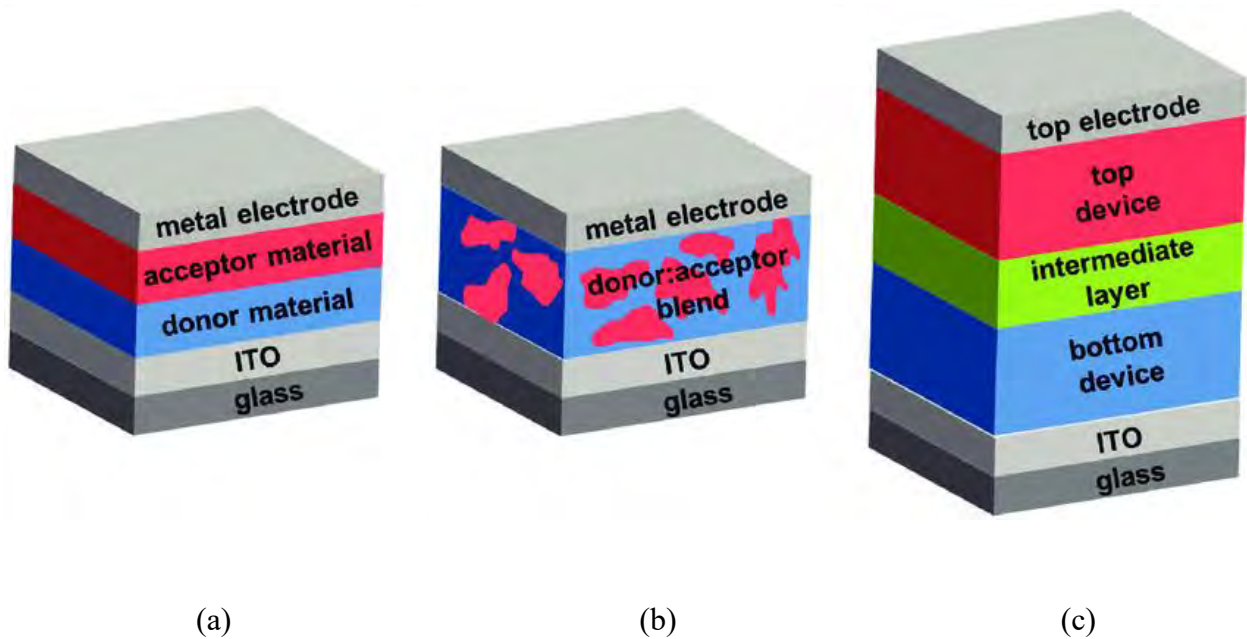
Figure 5: Different configurations for OSCs: a) planar heterojunction (PHJ), b) bulk heterojunction (BHJ), and c) tandem architecture. Here ITO is transparent electrode.

1.4.2 Charge Transportation and Collection

Upon creating of GEHP, electron resides in LUMO (lowest unoccupied molecular orbital) of acceptor while the hole stays in HOMO (highest occupied molecular orbital) of donor. The generated electron-hole pair are then swept away from the interface towards the electrode by a high electric field. The electric field is set up by the difference in work-functions of the two electrodes. The electric field can also be set up by creating a concentration gradient. The charges, in organic material, move from one localized state to another called hopping which results in a relative low charge carrier mobility [24]. Also, geminate recombination of electron-hole pair and bimolecular recombination of free carriers can occur in transportation path. Upon reaching the electrodes, the charges are collected. For efficient collection, the energy levels should be properly aligned i.e. the work-functions of the positive and negative electrode should be matched with the HOMO level of the donor and LUMO level of the acceptor respectively so that there lies minimum potential barrier.
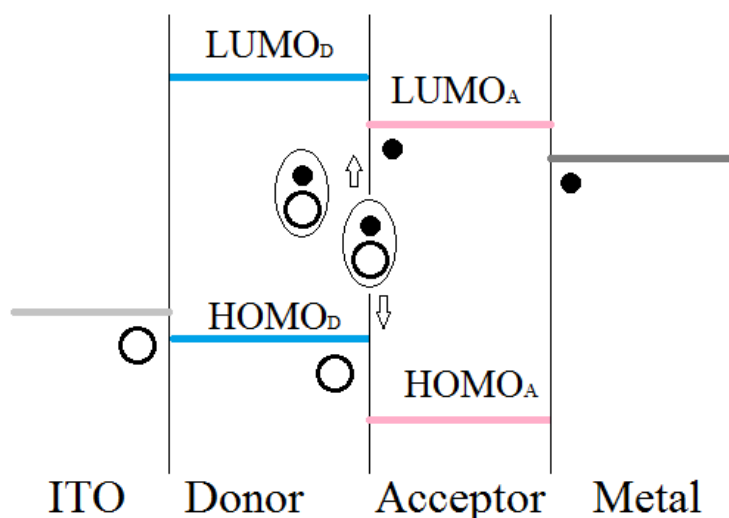
Figure 6: Energy level alignment of OSC. ITO and metal are the positive and negative electrodes respectively whereas black and white circles represent electrons and holes respectively.

1.5 Efficiency Enhancement Techniques of Solar Cell

Efficiency enhancement is the focal point in any solar cell research. Researchers have invented various techniques to improve the performance of the solar cell. The techniques involve pre and post processing of the solar cell in fabrication, enhancing light absorption or improving charge transportation mechanism.

1.5.1 Plasmonic Effect

For light absorption enhancement, a very common approach is to place 1D, 2D or 3D metallic nanostructures (MNS) inside the active layer [15], [16], [25], [26]. MNS increase light absorption inside the active layer by reflecting incident light from their surfaces. MNS also create localized surface plasmon resonance (LSPR) at particular wavelength. This phenomenon, referred to as plasmonic effect, increases light absorption manifold at the resonating wavelength and thus creating more carriers.

1.5.2 Upconversion

Upconversion is another technique to improve light absorption of solar cell [27] - [31]. The active material can absorb only the wavelengths with energy lower than the bandgap of the material. Wavelengths with higher energy than the bandgap remain unused. Most active materials can't absorb wavelengths after 1000 nm. For organic materials, the cut off wavelength is even lower because of higher bandgaps. The wavelengths after cut-off and energy associated with them are often termed as sub-bandgap losses. The sub-bandgap losses can be compensated by a technique called photonic upconversion. In photonic upconversion, the transmitted sun light is converted into a higher energy (higher frequency, lower wavelength) lights. The converted light can then be reflected back to the active material by simply placing a metal reflector below the upconverting

material. In this way, more energy can be harnessed inside the active medium. This will eventually increase the number of generated free carriers and the PCE of the solar cell. In any upconverison process, there is one or more sensitizer molecule(s) which are embedded with another type of molecule(s) (activator/annihilator) in a host matrix. The sensitizer molecules absorb unabsorbed sunlight and converts them into usable sunlight with the help of activators or annihilators. The host material, where the molecules are submerged, play an important role in determining overall efficiency of the upconversion process. Upconversion process can be broadly classified into two categories:

1. Two Photon Absorption (TPA)
2. Triplet-Triplet Annihilation (TTA)

1.5.2.1 Two Photon Absorption (TPA)

In two photon absorption, two different photons are absorbed by one or more rare earth doped upconversion materials and converted into a higher energy photon by one of four different ways namely, excited state absorption (ESA), energy transfer upconversion (ETU), photon avalanche (PA) and energy migration-mediated upconversion (EMU). In TPA, very high-power density (nearly 10-15 times solar irradiance) is required to excite sensitizer and activator molecules [32]. The theoretical upconversion efficiency of TPA is 50%.

1.5.2.2 Triplet-triplet Annihilation

In triplet-triplet annihilation process, two organic molecules interact with each other at their triplet states. This interaction leads one molecule excited to its emitting state and thus produces lower wavelengths. Light is initially absorbed by a sensitizer molecule and the molecule move to its

singlet excited stage S_1 as shown in figure 7. Then the sensitizer molecule moves to its triplet state T_1 because of molecular effect. At the same time, energy transfer to a neighboring molecule, called annihilator, excites the molecule to its triplet state as well. After this, two neighboring annihilators at triplet states interact. As a result of their interaction, one annihilator returns to lower state S_0 while the other is excited to a higher state S_1. A radiative decay of the late annihilator from singlet excited state to ground state produces upconverted light wave (fluorescence). TTA process needs very low power density to excite sensitizer and annihilator molecules (comparable magnitude to that of solar irradiance) [32]. The highest reported efficiency of TTA process is over 30% [33], [34]. Upconversion can also be realized by using quantum nanostructures. By designing compound semiconductor nanocrystals, upconversion in PV cells can be achieved.
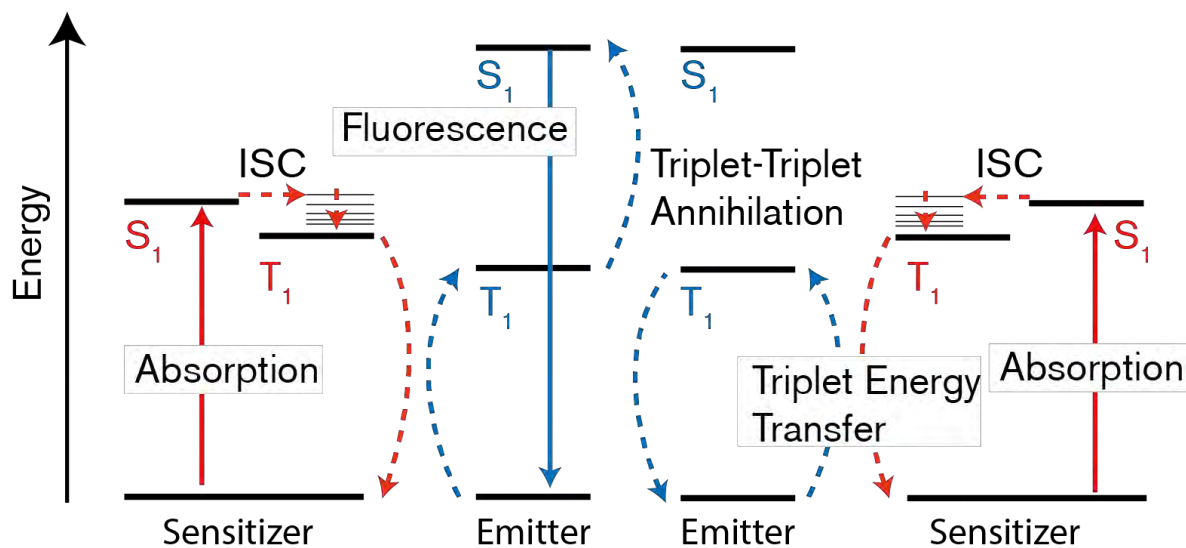
Figure 7: Triplet-Triplet Annihilation (TTA) process involving sensitizer and annihilator molecules.

1.6 Literature Review

Organic solar cell was first introduced in 2001 when Shaheen et. al. achieved an efficiency of 2.5% with an organic material named MDMO-PPV:PCBM [35]. Their success initiated organic solar cell research and researchers came up with various promising active materials over the years namely, P3HT:PCBM, PCPDTBT:PCBM, PTB7:PCBM etc. [36] - [38]. Polythiophene (PT) and its derivatives were and are still very popular homoconjugated electron donors in BHJ architecture which yield 3.5-4.5% efficiency [39], [40]. For achieving higher efficiencies of 5-7% [41], [42], polymers with 2,1,3- benzothiadiazole (BT based polymer), benzo[1,2-b;4,5-b']- dithiophene (BDT based polymer) have been developed in recent past. There are also a number of different polymer groups (DPP etc.) which have been tried in D/A structures. Till now, the maximum achievable efficiency of a single junction organic solar cell is around 10.47% [43]. The low value of PCE in organic solar cell (OSC) is mainly because of the poor absorption profile of organic materials in near-infrared regions (NIR) of solar spectrum as well as less efficient charge transportation mechanism.

A good number of theoretical analysis as well as experimental works on OSCs have been carried out by different research groups in recent years [35]-[48]. Among the different configuration of OSCs, bulk heterojunction (BHJ) OSCs have been reported to be the most promising structure [35], [36]. On the theoretical part, modeling of BHJ OSCs have been mainly done numerically over the years for practical purposes. There has been some analytical works reported in literature also [40], [44], [45]. To improve the efficiency of BHJ OSCs, different groups have tried different techniques experimentally such as addition of nanostructures and/or an extra layer [15], [26], [46] - [48]. Chi et.al [46]modified the OSC structure by placing an extra PCBM layer under the active layer and enhanced the efficiency from 3.6% to 4.24%. Jung et.al [26] placed a molybdenum layer

under the active P3HT:PCBM layer and added silver nano-particles on it for efficiency enhancement. Similarly, study with silver nano-particles has been carried away by other research groups as well [16], [47], [48]. Xuanhua et. al. [47] used patterned active layer together with silver nano-grating arrays and found enhanced light absorption and fill factor. Recently, there have been attempts to improve the performances of P3HT:PCBM by inserting nanostructures in between active layer and buffer layers [15], [16]. Although some investigations on nanostructure incorporation in and out of active layer have been performed, complete optoelectronic study on optimizing nanostructure incorporated organic solar cells have seldom been reported. The only related work, to the best of our knowledge, has been carried out by Fallahpour et.al. [25]. They have optimized the back-contact grating and improved the performance up to 17.5%.

A less used technique to improve power absorption in NIR and IR region is upconversion. Upconversion in solar cell has been studied both numerically and experimentally [49] - [52]. However, analytical model of upconversion in solar cell has hardly been reported. Upconversion has been previously employed in c-Si solar cells, where single Er^{3+} doped upconverting material in $NaYF_4$ microcrystal exhibited 5.1% upconversion efficiency at 1523 nm [27]. The recorded emissions at 1523 nm wavelengths were 550, 660, 800 and 980 nm, all of which falls below the cut off wavelength of Si (1100 nm). Similarly, in a-Si:H solar cell with Er^{3+} doped β-$NaYF_4$ upconverting (UC) layer displayed an enhanced current of 0.56 µA when simultaneously excited with 980 nm and 1560 nm [31]. For GaAs solar cell with UC layer, a PCE of 2.5% was achieved under 891 nm illumination [53]. There have been several reports where UC layer have been incorporated in OSCs as well. Wang et.al. used LaF_3:Yb^{3+}/Er^{3+} phosphors to obtain an upconverted current density of 16.5 µA/cm^2 at 975 nm illumination for P3HT:PCBM based single junction OSC [29]. With different host matrix ($NaYF_4$), Wu et.al. observed a short circuit current enhancement

of 0.5 μA for same OSC in 2012 [30]. Adikari et.al. showed and reported a maximum photo current density of 16 μA/cm^2 for PCDTBT:PCBM based OSC incorporating Y_2BaZnO_5:Yb^{3+}/Ho^{3+} by improving power absorption in between 870-1030 nm [28]. The highest recorded efficiency of upconversion process when used in solar cell is 16.7% [54].

1.7 Objective of the Thesis

The specific objectives of this thesis are:

- To model upconversion mechanism and study the effects of different upconverter layers on the PCE of bulk hetero-junction (BHJ) OSC with different active layers and cell topologies.

- To study the effects of concentrated sunlight on the upconversion process in OSCs and evaluate their performance.

- To find an optimized nano-plasmonic structure for improving the efficiency of BHJ organic solar cell.

- To increase the efficiency of BHJ OSC by utilizing the outcomes of the above studies.

1.8 Thesis Overview

This thesis is divided into four chapters.

Chapter 1 provides general introduction followed by necessary background, literature review and the objectives of the work.

Chapter 2 presents the methodology used for opto-electronic Modeling of BHJ OSCs'. Then it discusses the FDTD Modeling of upconversion process and a technique to study the effect of concentrated sunlight in solar cell performance.

The results obtained from the derived model are discussed in chapter 3. Variation of OSC efficiency with active layer thicknesses for transparent electrode and non-transparent electrode has been discussed. Then results obtained by incorporating an optimized upconverting layer have been elaborated. Finally, a highly efficient OSC has been designed by incorporating optimized nanostructure and a upconverter layer.

Chapter 4 contains the concluding remarks along with suggestions for future work on the topic.

Chapter 2

Methodology and Modeling

2.1 Device Structure

For comprehensive study on upconversion process, four different active materials namely, P3HT:PCBM, PSBTBT:PCBM, PBDTTT-C:PCBM and PTB7-Th:PCBM with BHJ architecture have been considered. As for structural configuration, both conventional (S1) and inverted (S2) OSC structures have been used. For both structural configuration and each active material, a 120 nm thick transparent conductive oxide indium tin oxide (ITO) has been used as top contact and a 200 nm thick Aluminum (Al) (conventional)/ Silver (Ag) (inverted) layer as bottom contact. For conventional structure, a 50 nm thick hole transport layer (HTL), namely, PEDOT:PSS has been used. For inverted structure, a 30 nm electron transport layer (ETL) namely, ZnO and a 10 nm hole transport layer (HTL) MoO_3 have been used. To incorporate UC layer in the S1 or S2 structure, the bottom contact has been replaced with a 100 nm thick transparent contact ZnO:Al. Then a 500 nm thick UC layer (host material) has been added where sensitizer and annihilator/activator molecules are embedded. Finally, the structure (S3 or S4) is completed with a perfect metal back reflector.
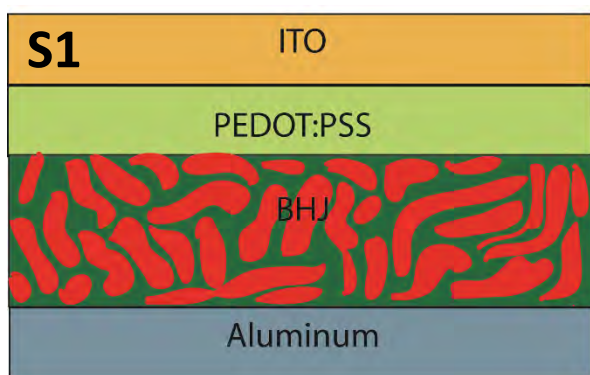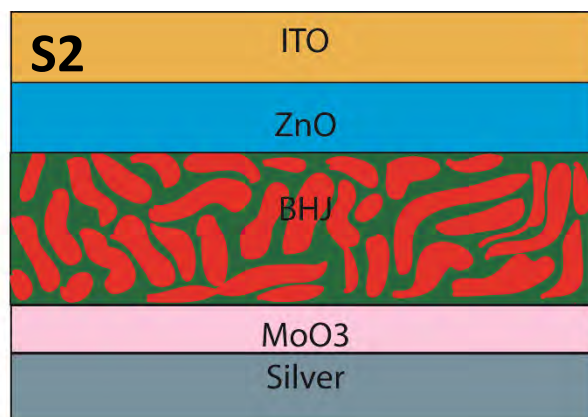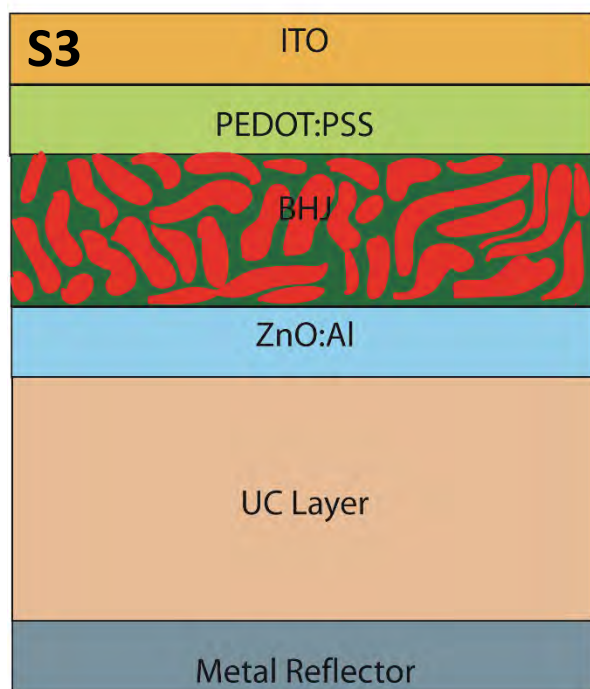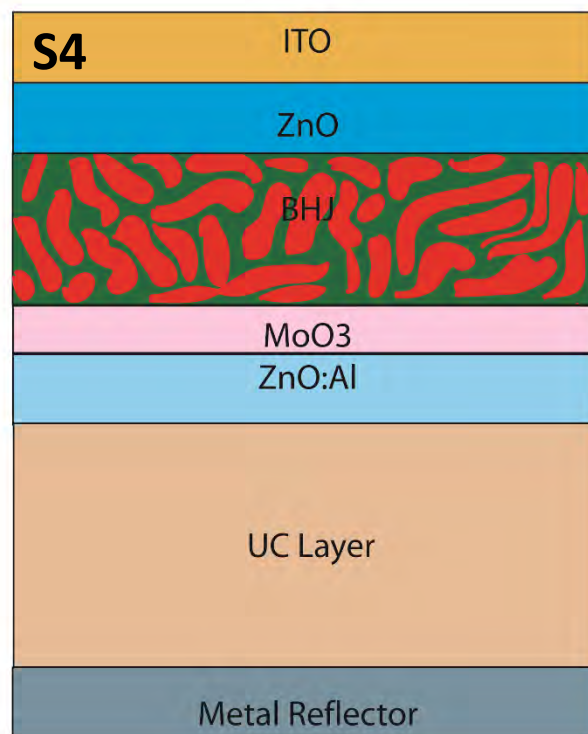
Figure 8: Device structures of organic solar cell: (a) S1 (b) S2 (c) S3 (d) S4. S1 is a conventional structure of OSC (ITO / PEDOT:PSS / BHJ / Al) whereas S2 is an inverted structure (ITO / ZnO / BHJ / MoO_3 / Ag). In structure S3, the metal electrode of S1 is replaced by a transparent electrode ZnO:Al followed by an UC layer and a metal reflector (ITO / PEDOT:PSS / BHJ / ZnO:Al / UC layer / Reflector). In S4, the aforementioned process has been followed for the inverted structure S2 (ITO / ZnO / BHJ / MoO_3 / ZnO:Al / UC Layer / Reflector).

2.2 Methodology

The methodology used in this has been depicted in the following block diagram:

| Drawing the solar cell geometry | ⇨ | Calculating optical electric field distribution using a FDTD solver | ⇨ | Estimating the power absorbed in the active medium using Poynting theorem | ⇨ | Calculating ideal short circuit current density from the power absorption profile |

⇩

Calculating the carrier generation rate of the solar cell

⇩

| Estimating PCE of the solar cell | ⇦ | Determining J_{SC}, V_{OC} and FF of the solar cell | ⇦ | Solving drift-diffusion equation, Poisson equation and continuity equation to find solar cell I-V characteristics |

⇩

| Modifying the geometry for upconversion | ⇨ | Determining power absorbed in the upconverted layer using spectral parameters | ⇨ | Calculating upconverted short circuit current density from the power absorption profile | ⇨ | Estimating PCE of the upconverted solar cell |

Figure 9: Methodology for opto-electronic modeling of solar cell with upconverter layer. The solid outlined blocks represent methodology for optical modeling. The dashed blocks represent methodology for electrical modeling whereas the dotted blocks represent methodology to describe upconversion is solar cell.

The methodology for nanostructure modeling and concentrated sunlight modeling have not been shown separately since same opto-electronic modeling scheme have been used for both cases.

Complete optoelectronic modeling of organic solar cell is necessary to evaluate OSCs performance. Optical behavior of OSCs is similar to any other solar cells (except exciton creation and separation) where absorbed optical power is converted to free electrical charges (excitons and consequently electron-hole pair in OSC). The optical power absorbed per unit volume (P_{abs}) is dependent on the refractive index profiles of the active material and can be formulated as Eq. (4) for a monochromatic source of wavelength λ.

$$P_{abs}(x,\lambda) = -\frac{\pi c}{\lambda} \times E(x,\lambda)^2 \times Im\big(\varepsilon(x,\lambda)\big) \qquad (2.1)$$

where E is position and wavelength dependent electric field, $Im\big(\varepsilon(x,\lambda)\big)$ is the imaginary part of the permittivity which is also position (material) and wavelength dependent. The number of generated excitons can be approximated to be equal to the number of absorbed photons if the internal quantum efficiency is assumed to be unity. With the assumption, the generation rate can be calculated simply by dividing Eq. (4) with the energy of single photon.

$$G(x,\lambda) = \frac{P_{abs}(x,\lambda)}{h\upsilon} \qquad (2.2)$$

where h is Planck constant and υ is frequency of light. For sunlight, having a range of frequencies, the total generation rate can be calculated by integrating the generation rate profiles with respect to the wavelengths (Eq. (6)).

$$G(x) = \int G(x,\lambda)d\lambda \qquad (2.3)$$

where, $G(x,\lambda)$ is the position dependent generation rate for single wavelength and $G(x)$ is the generation rate profile considering all wavelengths i.e for a broadband source (sunlight). Generated excitons get separated under the influence of the internal electric field within their diffusion range. The motion of free charge carriers (electron and hole) is described according to the drift diffusion equations [Eqs. (7) and (8)].

$$J_n = qn\mu_n E + qD_n\nabla n \qquad (2.4)$$

$$J_p = qp\mu_p E - qD_p\nabla p \tag{2.5}$$

where, here and in what follows, *J* is current density for different charges, n and p are electron and

hole densities, μ and *D* are charge mobility and diffusion coefficient respectively. The subscripts

'n' and 'p' in *J*, μ and *D* represent electron and hole quantities respectively. The generated electrons

and holes travel to respective electrodes where they are collected and power flows to the external

circuit. However, some electrons and holes do recombine before reaching the electrodes and reduce

the collection efficiency. The generation, recombination and collection of charges cause the carrier

concentration to change continuously inside the active material following the charge conservation

law. This is modelled by the set of continuity equations (Eqs. (9) & (10)).

$$\frac{dn}{dt} = -\frac{1}{q} \times \nabla J_n - R_n + G_n \tag{2.6}$$

$$\frac{dp}{dt} = +\frac{1}{q} \times \nabla J_p - R_p + G_p \tag{2.7}$$

where R and G are recombination and generation terms, respectively. Finally, the potential variation

inside the active material can be determined by solving Poisson equation (Eq. (11)).

$$-\nabla \varepsilon E = q(p - n + N_D - N_A) \tag{2.8}$$

where N_D and N_A are doping densities. The distribution of current densities (J_n and J_p) needs to be

calculated for deriving J-V characteristics. And the densities are calculated by solving Eq. (7) to

(11) simultaneously. From J-V characteristics, PCE can be obtained by Eq. (12).

$$\eta = \frac{V_{oc} J_{sc} FF}{P_{in}} \tag{2.9}$$

Where, P_{in} is power of solar spectrum (100 mW/cm^2 for AM1.5 solar spectrum). Recombination

mechanism, which reduces the PCE (Eqs. (9)-(10)), can be classified into two types for organic

materials. The process of electron and hole recombination in organic materials can be described by

a theory named after physicist Paul Langevin and is called bimolecular recombination process [55], [56]. The recombination rate can be expressed by Eq. (13).

$$R_B = \frac{q}{2\varepsilon}(\mu_n + \mu_p)(np - n_i^2) \qquad (2.10)$$

where, n_i is the intrinsic carrier concentration and other symbols have their usual meanings. Another recombination process, monomolecular recombination, occurs when charge carriers meet a trap state with opposite sign. It is usually referred to as Shockley-Read-Hall (SRH) recombination and can be expressed by Eq. (14) [57].

$$R_M = \frac{np - n_i^2}{\tau_e(n + n_{traps}) + \tau_h(p + p_{traps})} \qquad (2.11)$$

where, τ_e and τ_h are trap lifetime and n_{traps} and p_{traps} are trap density of states.

For upconversion, the back contact or (metal electrode) must be replaced by semitransparent or transparent electrode so that light can be passed into the UC layer. In doing so, the unabsorbed or below bandgap photons will be transmitted to the UC layer. Assuming the spectral irradiance incident on upconverting layer $T_{UC}(\lambda)$ is known, total power absorbed by the UC layer can be calculated from Eq. (15).

$$P_{absUC} = \sum_{i=1}^{n} \int B_i(\lambda) T_{UC}(\lambda) d\lambda \qquad (2.12)$$

Where it's been assumed that the host matrix has n sensitizer molecule each having different absorption spectra $B_i(\lambda)$. The absorbed wavelengths will be converted into usable wavelengths by UC layer. If a metal reflector is placed after UC layer (S3 or S4 as reference), then the upconverted wavelengths will reflect back to the active layer through the transparent electrode where the recycled wavelengths will be available for absorption. Assuming that, the UC layer has an efficiency of η_{UC}, the emitted (upconverted) spectral irradiance, $H_{UC}(\lambda)$ can be estimated using Eq. (17).

$$\eta_{UC} P_{absUC} = \int_0^\infty H_{UC}(\lambda) d\lambda \qquad (2.13)$$

By analyzing absorption and emission spectra of experimentally realized sensitizer molecules, the absorption and emission spectra can be approximated to be a Gaussian distribution with peak absorbance being unity [51], [52], [58]. The peak value for emitted spectra will, of course, depend on the amount of the power absorbed by the UC layer and the efficiency of the process (P_{absUC} and η_{UC}). The spectra emitted by UC layer will be available for the active medium to absorb. The active medium will absorb fraction of the upconverted photons and new charge carriers will be generated in aforementioned process (Eqs. (4)-(6)). The new charge carriers will contribute to the original short circuit current density. The upconverted short circuit current density can be determined by replacing solar spectrum with emitted spectrum of UC layer in the definition of ideal short circuit current density (Eq. (18)).

$$J_{SCUC} = \frac{e}{hc} \int_0^\infty \lambda * A_{UC}(\lambda) * H_{UC}(\lambda) d\lambda \qquad (2.14)$$

where, $A_{UC}(\lambda)$ is the fraction of the upconverted photons absorbed by the active layer which is same as external quantum efficiency $EQE(\lambda)$. Finally, the overall efficiency can be estimated by adding the contribution of upconverted short circuit current density with the short circuit current density of cell with UC layer.

$$\eta = \frac{V_{OC}(J_{SC} + J_{SCUC})FF}{P_{in}} \qquad (2.15)$$

Two approximations have been made in developing the methodology of upconversion which will lead to slight over-estimation of FOMs. Firstly, $A_{UC}(\lambda)$ has been approximated as $P_{abs}(\lambda)$ instead of $EQE(\lambda)$. This will result in a slightly higher estimation in J_{SCUC} since carriers generated from upconverted photons may recombine. Since, the upconverted carriers are few, error from this approximation will be very low. Secondly, the values of V_{OC} and FF have been considered to be

24

same for both Eq. (12) and (19) where the equations represent the PCE of a solar cell without (S1 or S2) and with UC layer (S3 or S4) respectively. It is understandable that, the two solar cells may have different values of V_{OC} and FF. However, V_{OC} and FF largely depend on electrical characteristics which remain almost same for both cells. Even with these approximations, the results obtained from simulation agree well with the experimental values.

2.3 Modeling

The Modeling of OSC has been carried out using an integrated opto-electronic solver. Two separate but interconnected modeling methods, namely optical modeling and electrical modeling have been employed for simulating the solar cell. For optical modeling a commercial FDTD (Finite Difference Time Domain) solver has been used whereas for electrical modeling, a self-consistent charge transport solver has been used.

2.3.1 Optical Modeling

At first the structure is drawn by stacking the layers in z direction. Then, the real (n) and imaginary (k) components of refractive index parameters for each material have been provided as inputs [38], [43], [59], [60]. The refractive index profiles ($n(\lambda)$ and $k(\lambda)$) have been fitted with built-in fitting parameters in solver. A planewave source (AM1.5 solar spectrum) is placed over the top contact with wavelength range between 300-1600 nm. The source has been placed to point in z direction downward. A 2D FDTD simulation region is defined with periodic boundary conditions being employed in XY plane. PML (perfectly matched layer) conditions have been used in z directions near top contact to avoid reflection while metal boundary conditions have been used in z direction near bottom contact. The solver computes the optical electric field distribution ($E(x, \lambda)$) in the FDTD region by solving Maxwell's equation. The optical electric field distribution is used to

calculate the optical power absorbed by the cell and thus the carrier generation rate. This is manually done by using an analysis group which numerically calculate the optical power absorbed and carrier generation rate in the defined area (Eqs. (4)-(6)). For accurate estimation, an optimum 3 nm mesh is used in the active medium.

2.3.2 Electrical Modeling

Here again, the structure is drawn at first. Then electrical parameters (listed in Table 1 and 2) of each material are provided as inputs. The carrier generation rate from optical simulation is imported in electrical simulation. A simulation region is again defined covering the contacts. The contact layers are specified and a voltage sweep is added to generate J-V characteristics. Most importantly, two doping regions are defined near the contacts to create a built-in potential inside the active layer for charge sweeping. After simulation, carrier concentrations and densities inside the structure are obtained. By numerical manipulation, J-V characteristic curve is obtained from which the figure of merits (FOM) can be easily calculated.

2.3.3 Upconversion Modeling

To model upconversion, S3 and S4 structure (Figure 8(c)-(d)) have been used. In optical modeling, a flux monitor has been placed after the transparent electrode to measure the transmitted light i.e. sun light available to the UC layer for photonic upconversion. The UC layer has been modelled as a dielectric with refractive index n=1.5 and placed after transparent electrode. Then, the power absorption in the UC layer, emitted spectra from UC layer and upconverted short circuit current density have been optimized numerically using FOM obtained from electrical simulation.
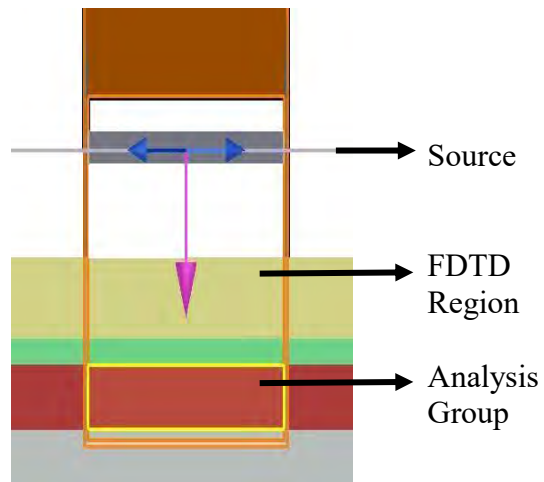
(a)
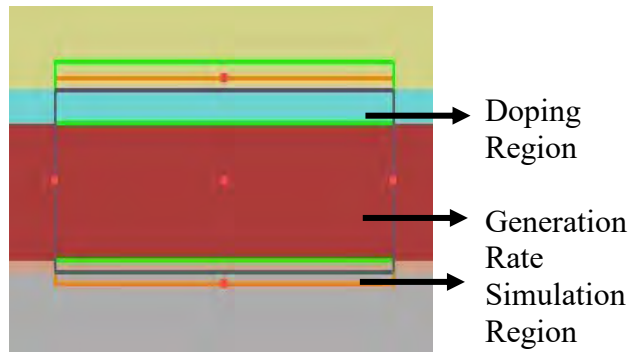
(b)
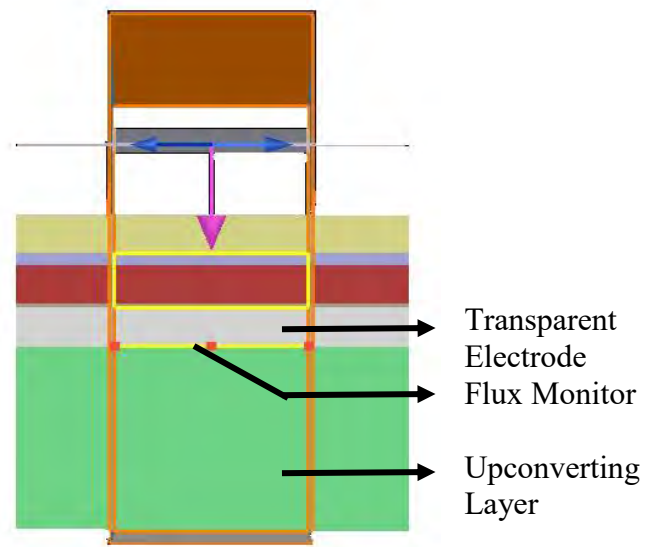
(c)

Figure 10: (a) Optical modeling of S1 (b) Electrical modeling of S3 (c) Upconversion modeling of S4.

2.3.4 Nanostructure Modeling

To introduce plasmonic effect, metallic nanostructures (MNS) have been incorporated in active layer. After which, simulations have been carried out with methodology and modeling described above. However, in optical Modeling, the absorptions in MNS have been forced to be zero since only active layer absorption will lead to carrier generation. Then plasmonic effects have been observed by inspecting the enhancement of optical electric field $E(x, \lambda)$ inside the active layer at different wavelengths. In electrical simulation, MNS have been left out from the active layer because of no generation rate in MNS region (due to no absorbance).

2.3.5 Concentrated Sunlight Modeling

For concentrated sunlight modeling, the solar irradiance has been multiplied by the concentration factor (C) and optical simulations have been carried away. The generation rate obtained from optical simulation has been provided as input in electrical simulation (similar to section 2.3.2) and the simulation has been performed. Finally, the equation for PCE estimation (Eq. 12) has been modified (multiplying the input power with C).

Chapter 3

Results and Discussion

To demonstrate the effect of UC layer on OSC, four different active materials having different PCE ranges have been chosen. For each OSC (S1 or S2 structure), the active layer thickness has been varied and an optimum thickness (and PCE) have been recorded. Then, the metal electrode in (S1 or S2) structure has been replaced with a transparent electrode and the resulting S3 or S4 configuration has been simulated with varying thicknesses. For the S3 or S4 structure at optimum thickness, the upconverter quantum yield of an optimized UC layer (optimized spectral characteristics) has been varied to observe its effect in PCE enhancement. The aforementioned process has been followed for four different organic materials and significant PCE enhancement has been observed in each case.

Among the four materials tried, metallic nanowires (MNWs) have been incorporated in the active medium of most efficient material. The MNWs dimensions have been optimized to introduce plasmonic effect inside the active medium. Then, at optimized thickness and MNW dimension, an efficient and optimized UC layer has been used to increase the PCE furthermore. Finally, effect of concentrated sunlight has been studied for the most efficient structure.

3.1 Benchmarking

To verify the simulation environment, J-V characteristics of each material as well as the upconversion process has been benchmarked with experimental results and models available in literature. Table 1 and 2 list the parameters that have been used to model, benchmark and study the solar cells. Figure 11 depicts the energy level alignments of the solar cells. Comparison of FOM with literature for benchmarking are listed in Table 3 and 4 with corresponding figures in Figure 12 and 13. Table 3 compares the FOM parameters obtained from simulation and FOM reported in literature for four different active materials used in this thesis. A root mean square error (RMSE) has been calculated for each material based OSC by comparing JV characteristics obtained from model and reference. The RMSEs have also been listed in Table 3. The corresponding JV characteristics have been depicted in Figure 13. From Table 3 and Figure 12, it can be concluded that the opto-electronic simulation environment created in the model is satisfactory.

Table 1: Parameters used in electrical simulation of OSC.

Materials / Parameters		P3HT :PCBM [39], [40]	PSBTBT :PCBM [61], [62]	PBDTTT-C :PCBM [42], [60], [63]	PTB7-Th :PCBM [64], [65]	PEDOT :PSS	ZnO [66]	MoO$_3$ [67]
LUMO (eV)		4.2	4.2	4.2	4	3.5	4.3	2
HOMO (eV)		5.2	5.05	5.16	5.2	5.1	7.7	5.05
Bandgap (eV)		1	0.85	0.96	1.2	1.6	3.4	3.05
Mobility (cm^2/Vs)	Electron	0.003	0.03	0.01	0.0008	0.77	150	3000
	Hole	0.0002	0.003	0.01	0.001	0.77	50	3000
Density (/cm^3)	Donor	1e20	5e17	5e21	1e17	-	-	-
	Acceptor	1e20	5e17	5e21	1e17	-	-	-
Lifetime (µs)		4	0.004	0.2	0.6	-	-	-
Langevin Constant (cm^3/s)		e-10	e-9	e-10	e-11	-	-	-
Permittivity		3.4	3.8	3.8	3.5	3	8.5	18

Table 2: Workfunction of electrodes used.

Electrode	ITO	Ag	Al
Work function (eV)	4.8	4.2	4.28

ITO (+)   PEDOT:PSS   P3HT   PC$_{60}$BM   Al (-)

-3.3 eV
LUMO

-4.2 eV
LUMO   -4.3 eV

-4.8 eV
-5.1 eV   Eg
-5.2 eV
HOMO

- 6 eV
HOMO

(a)

ITO (+)   PEDOT:PSS   PSBTBT   PC$_{60}$BM   Al (-)

-3.27 eV
LUMO

-4.2 eV
LUMO   -4.3 eV

-4.8 eV   Eg
-5.1 eV   -5.05 eV
HOMO

- 6 eV
HOMO

(b)

ITO (+)   PEDOT:PSS   PBDTTT-C   PC60BM   Al (-)

-3.35 eV
LUMO

-4.2 eV
LUMO   -4.3 eV

-4.8 eV   Eg
-5.1 eV
-5.16 eV
HOMO

- 6 eV
HOMO

(c)

ITO (-)　　　　ZnO　　　　PC$_{70}$BM　　　　PTB7-Th　　　　MoO$_3$　　　　Ag (+)

-3.6 eV
LUMO

-4.0 eV
LUMO

-4.3 eV

-4.2 eV

-4.8 eV

Eg

-5.05 eV

-5.3 eV
HOMO

- 5.9 eV
HOMO

(d)
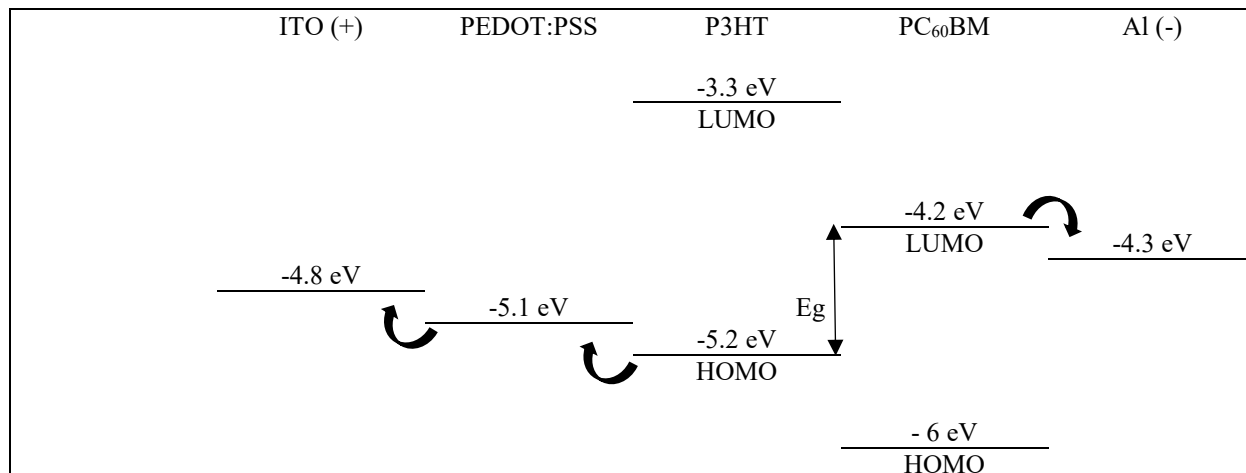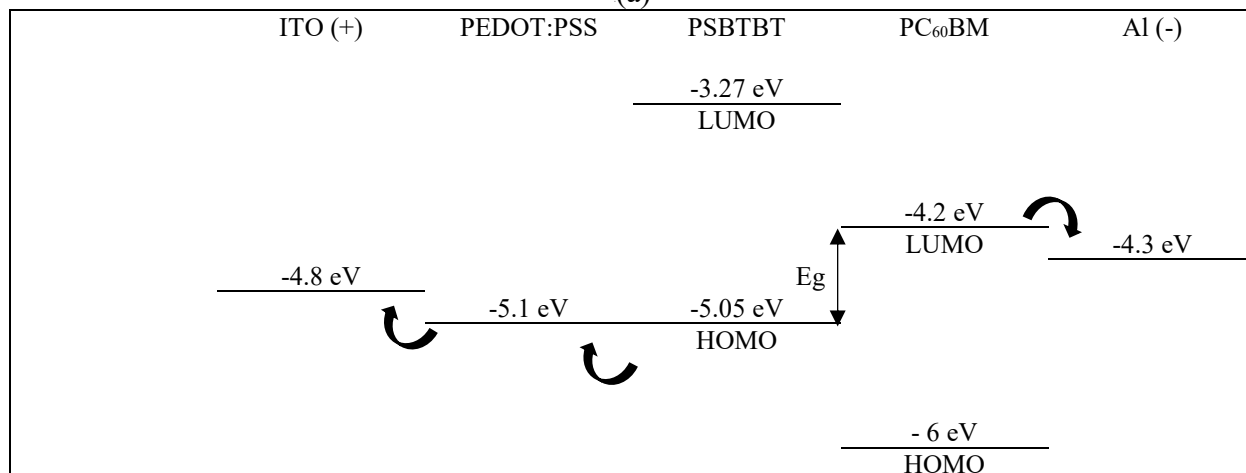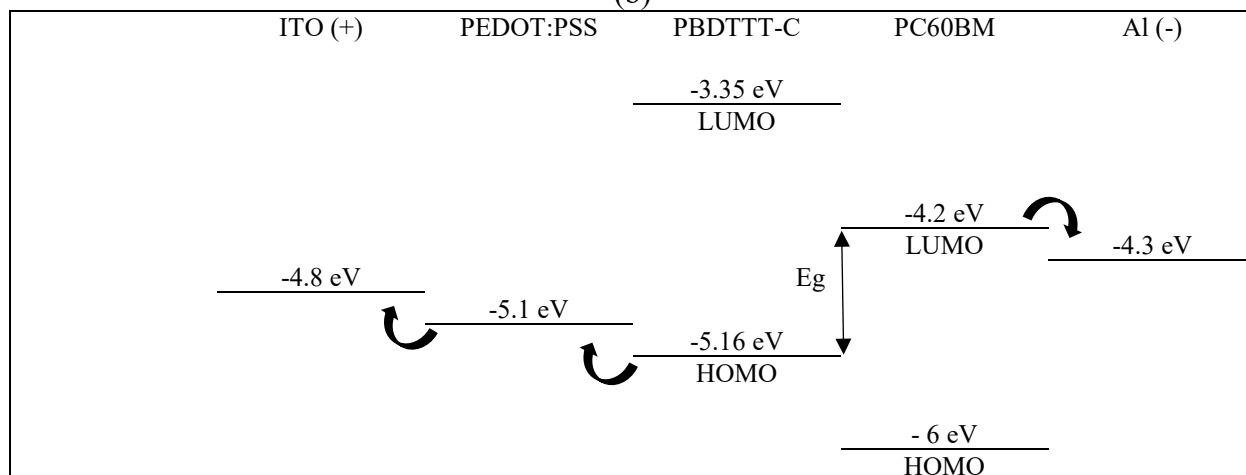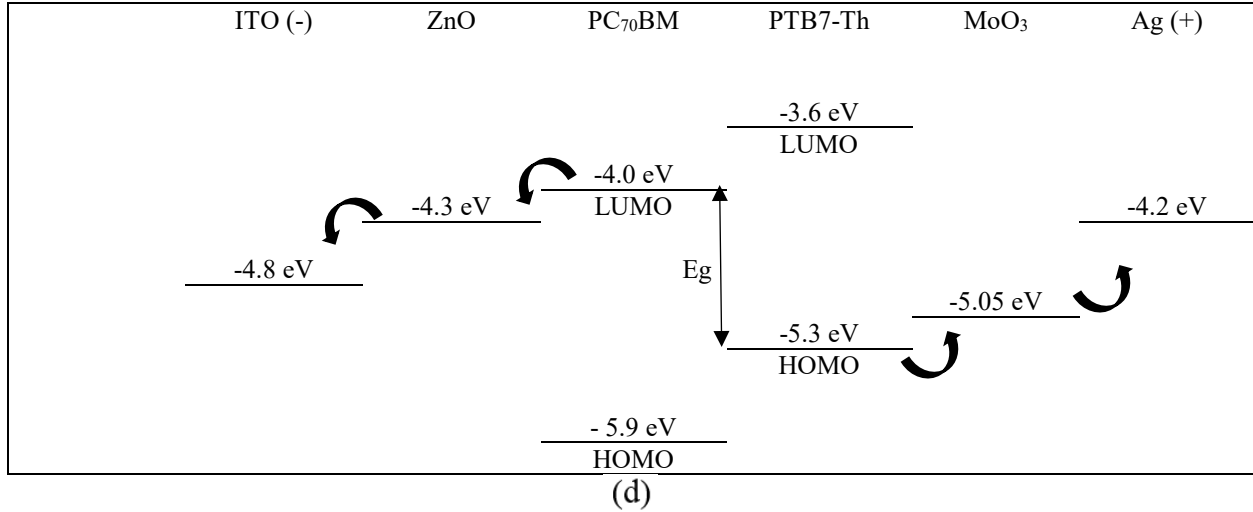
Figure 11: Energy level alignments of (a) P3HT:PCBM (b) PSBTBT:PCBM (c) PBDTTT-C:PCBM and (d) PTB7-Th:PCBM based organic solar cells.

Table 3: Comparison of figure of merits in benchmarking simulation model with references for four active materials

Material Name	Thickness (nm)		PCE, η (%)	Open Circuit Voltage, V_{OC} (V)	Short Circuit Current Density, J_{SC} (mA/cm^2)	Fill Factor, FF (%)	JV Curve RMSE, (%)
P3HT: PCBM	100	Model	4.29	0.597	10.22	70.40	7.3985
		Ref. [39]	4.31	0.597	9.69	74.45	
PSBTBT: PCBM	80	Model	5.02	0.689	12.92	56.34	6.4779
		Ref. [61]	5.10	0.680	12.70	50.00	
PBDTTT-C: PCBM	100	Model	6.34	0.695	13.74	66.47	1.7418
		Ref. [42]	6.3	0.711	14.10	63.00	
PTB7-Th: PCBM	80	Model	10.55	0.768	19.06	72.07	3.696
		Ref. [64]	10.30	0.782	19.50	67.60	
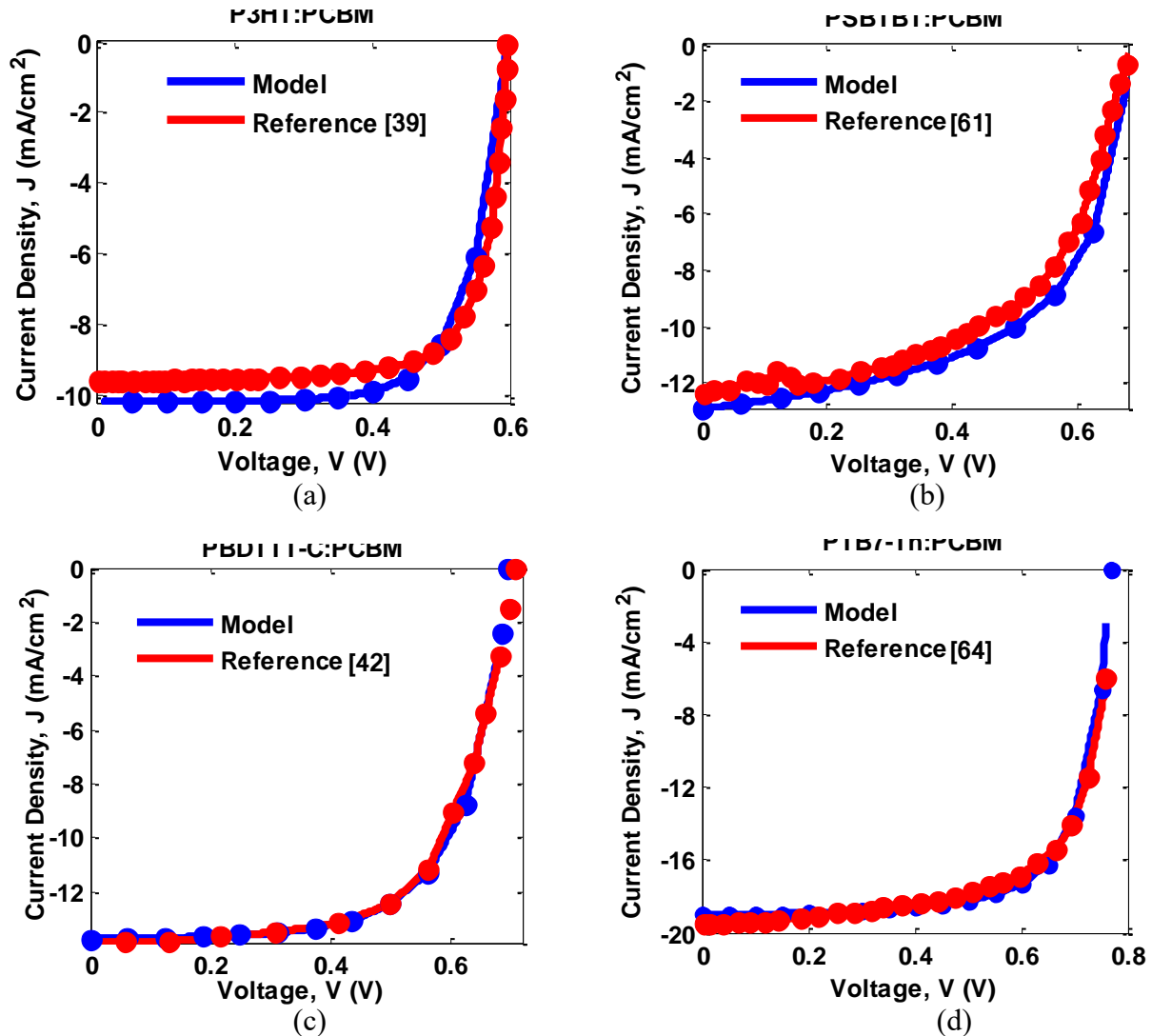
Figure 12: JV characteristics benchmarking of (a) P3HT:PCBM (b) PSBTBT:PCBM (c) PBDTTT-C:PCBM (d) PTB7-Th:PCBM based OSC having S1, S1, S1 and S2 configuration. The blue lines indicate values obtained from simulation model and red lines mark the values extracted from experimental and analytical works in literature. The blue circled markers refer the simulations points. The solid line does not represent results rather provides a guide to eye.

Table 4 lists the spectral parameters i.e. the peak position as well as the full width half maximum (FWHM) of absorption and emission spectra used to model the upconversion process reported in literature. It is noteworthy, that the upconversion model developed in this thesis is capable of handling multiple absorption spectra at a time but only one emission spectra. So, most dominant emission spectrum (located at 550 nm) has been used to model the upconversion process while the

33

other emission spectra have been discarded. Also, FWHM of absorption spectra has been undefined in the report. So, a standard FWHM of 25 nm was assumed for conservative estimation.

Table 4: List of spectral parameters used to benchmark upconversion process having 0.19% efficiency

	Absorption Peak (nm)	Absorption FWHM (nm)	Emission Peak (nm)	Emission FWHM (nm)	Increase in Photocurrent Density, J_{SCUC} (μA/cm^2)
Ref. [28]	975	Unspecified	525, 550, 675	25, 50, 20	16.5 (14 sun)
Model	975	25	550	50	1.1537 (1 sun)
					16.1518 (14 sun)
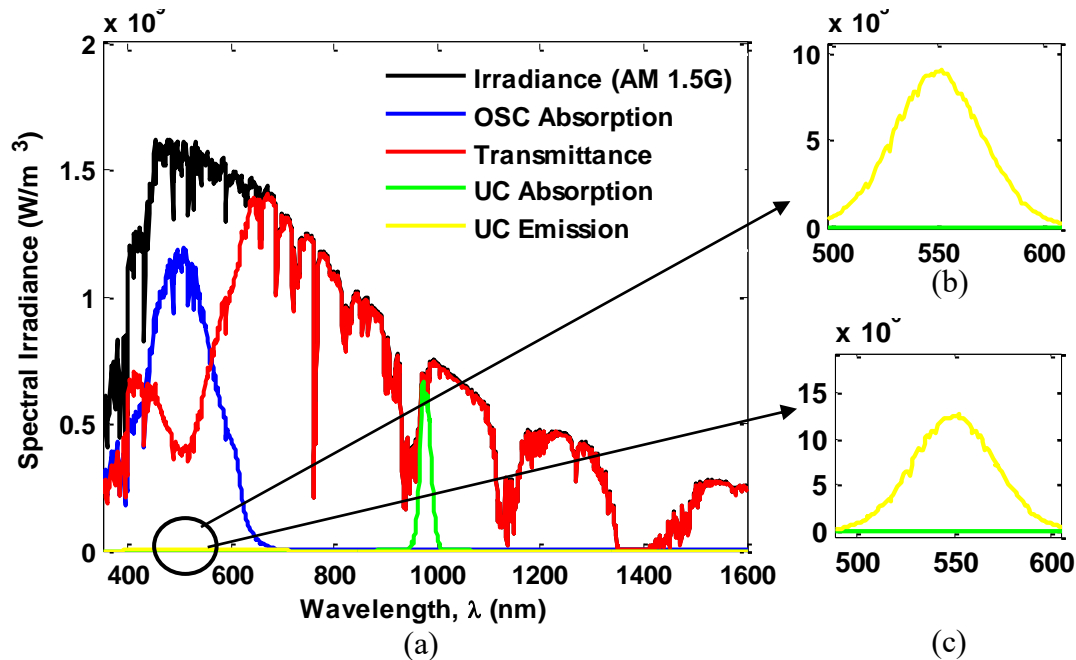
Figure 13: (a) Spectral irradiance of reference structure generated using upconverter model. Magnified version of (a) in 500 - 600 nm wavelength range for observation of UC emission is shown for (b) 1 sun illumination (c) 14 sun illumination.

3.2 Effect of Upconversion in OSC

The effect of upconversion on four different active materials, namely P3HT:PCBM, PSBTBT:PCBM, PBDTTT-C:PCBM and PTB7-Th:PCBM have been discussed in this section.

34

3.2.1 P3HT:PCBM Based OSC

To study the effect of upconversion process on P3HT:PCBM, thickness of P3HT:PCBM layer in conventional structure (S1) has been varied from 60 nm to 220 nm to estimate maximum PCE that can be achieved without upconversion. Then, similar study has been carried out for S3 structures. Finally, effect of an UC layer (with optimized characteristics) on most efficient S3 structure has been predicted.

For conventional structure, the highest efficiency has been noted at 80 nm thickness where PCE reaches up to 4.55% with J_{SC} = 10.31 mA/cm^2, V_{OC} = 0.608 V and FF = 72.62%. With increasing thickness, power absorption inside the active layer increases which leads to more carrier generation. However, the recombination processes also become dominant with increasing thickness as carriers have to travel longer distances before reaching electrode (Figure 14 (d)). So, there lies an optimum thickness for which the efficiency is maximized. It is evident from Figure 14 (c) that the thickness has very little effect on the open circuit voltage. When the metal electrode is replaced with a transparent ZnO:Al layer, the PCE at all thicknesses decreases. This is understandable since transparent electrode can not facilitate sunlight reflection towards the active layer like the metal electrode. A maximum PCE of 3.23% has been obtained for 200 nm thick active layer incorporated trasnparent cell with J_{SC} = 10.19 mA/cm^2, V_{OC} = 0.576 V and FF = 55.06%.

With 200 nm P3HT:PCBM layer, the S3 structure absorbs wavelengths up to 650 nm consuming approximately 36.0 mW/cm^2 solar power (total solar power = 100 mW/cm^2). A massive 63.0 mW/cm^2 power (from 700 nm wavelengths on wards) has been found to be unabsorbed by the cell as depicted in Figure 13 (considering a minute loss accounted in ZnO:Al). To absorb a fraction of

the unused solar power, an UC layer has been placed after the trasnparent electrode followed by a metal reflector. Sensitizer molecules placed in the UC layer can absorb wavelegths after 700 nm. With the help of activcator (TPA) or annihilator (TTA) molecules, it UC layer can later emit smaller wavelengths ($\leq$ 650 nm) after internal atomistic and chemical process. The smaller wavelengths will reflect back towards the active layer by the metal reflector through ZnO:Al and will be absorbed by the active layer. In this way, more light will be harvested and more carreirs will be generated. Eventually, the generated carriers will contribute to higher PCE. The amount of light harvesting will entirely depend on the absorbing and emiting wavelengths. Different types of sensitizer molecules will absorb power from different region of the unused spectrum. More sensitizer molecules with complementary absorption profiles will be able to harness more power from unused spectrum. The active material has different power absorption intensity at different wavelengths. So, it is important that the active layer has good power absorbtion at emititng wavelength from UC layer. The upconverter model developed in this thesis can facilitate multiple absorption but only single emission

For P3HT:PCBM based OSC, an UC layer with three different sensitizer molecules have been proposed. The absorption peaks of three sensitizers as well as emission peak have been simultaneously optimized (listed in table 5). The FWHM of absorption peak has been considered to be 100 nm whereas an emission FWHM has been kept fixed at 25 nm. The standard FWHM of absorbers in upconversion is 50 nm. However, the highest reported FWHM for an absorberis 125 nm and the lowest reported emission FWHM is 12 nm. With optimized absoption and emission spectra, the quantum efficiency of the UC layer has been varied to predict the PCE and upconverted current density of the entire cell.
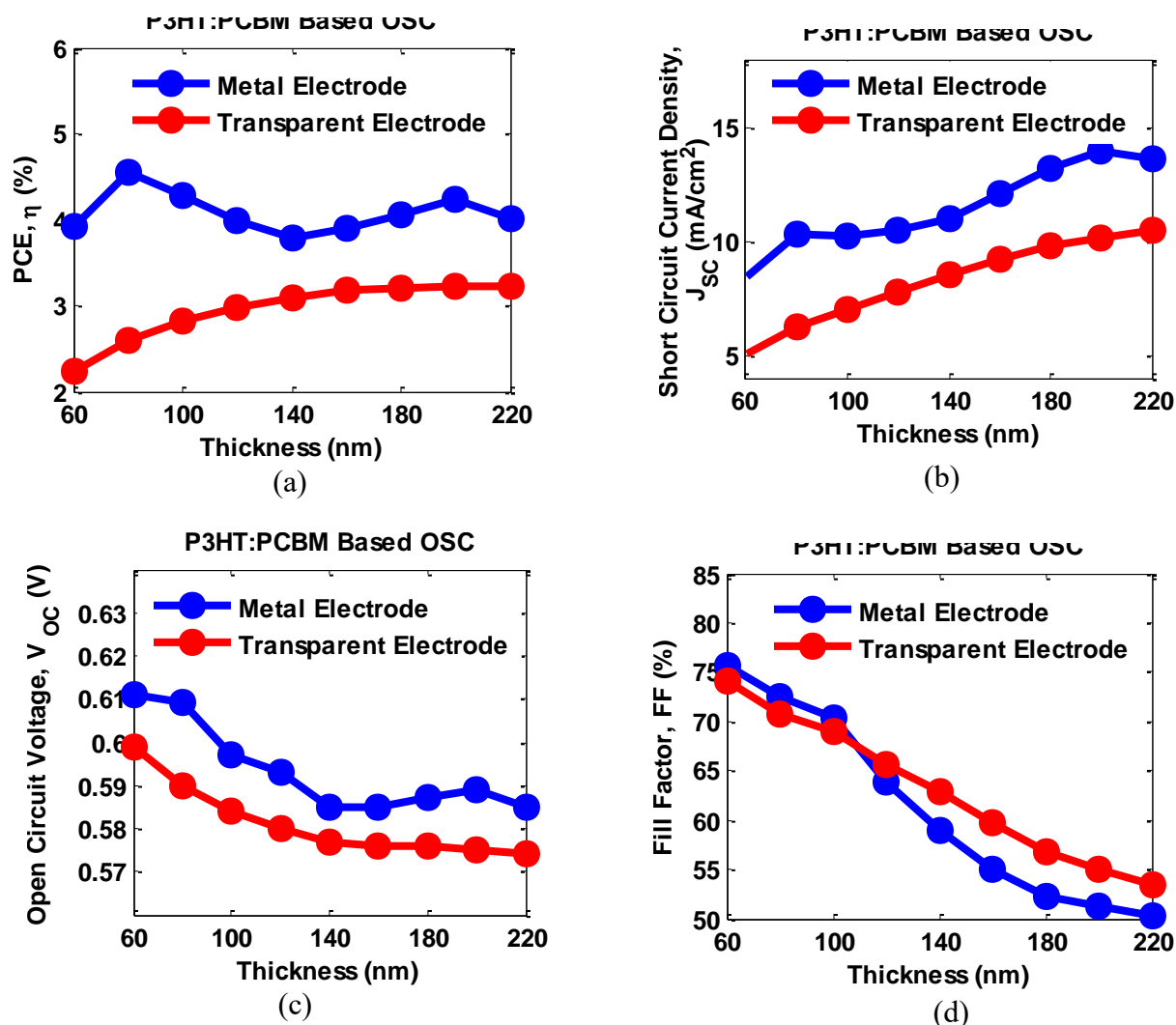
Figure 14: Variation of (a) Power Conversion Efficiency (PCE) (b) Short Circuit Current Density (c) Open Circuit Voltage and (d) Fill Factor with active layer thickness for conventional (S1) and transparent structures (S3) of P3HT:PCBM based OSC. The blue and red circled markers represent simulation points. The solid lines do not refer to results rather provides a guide to eye.

Table 5: Optimized parameters of absorber and emitter molecules spectral characteristics for P3HT:PCBM based S3 structure.

Molecule	Peak Position (nm)			FWHM (nm)
Sensitizer (Absorber)	695	751	1017	100
Annihilator (Emitter)	530			25
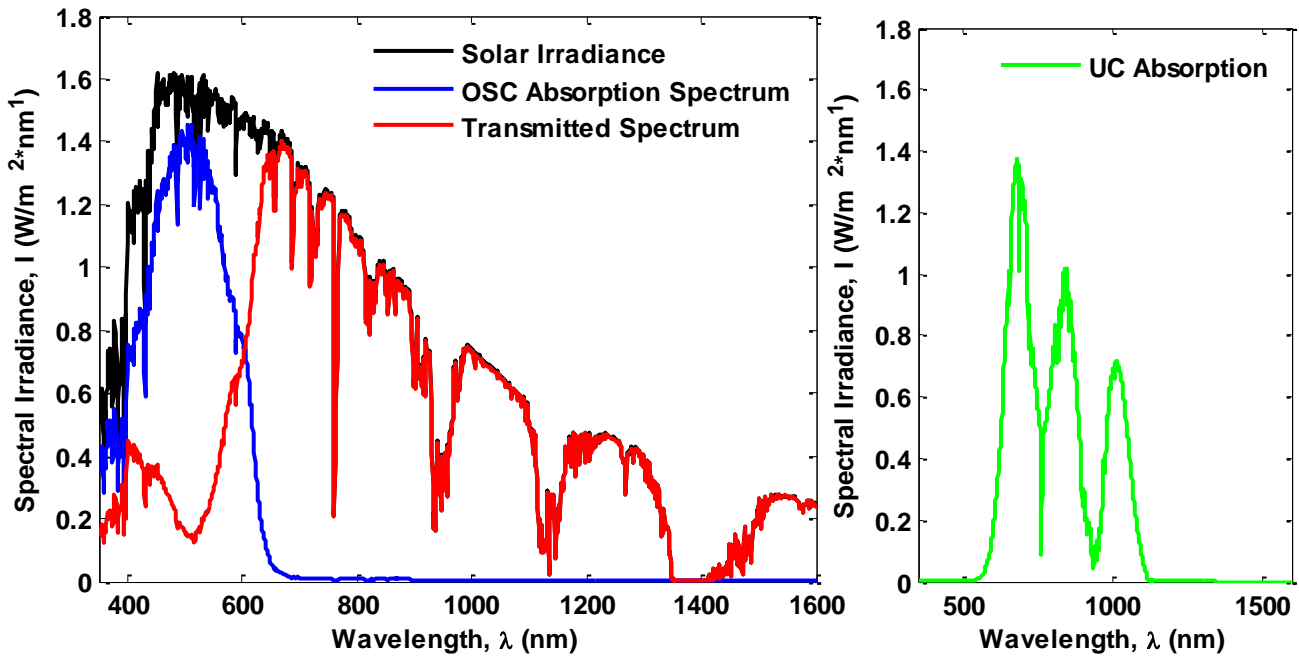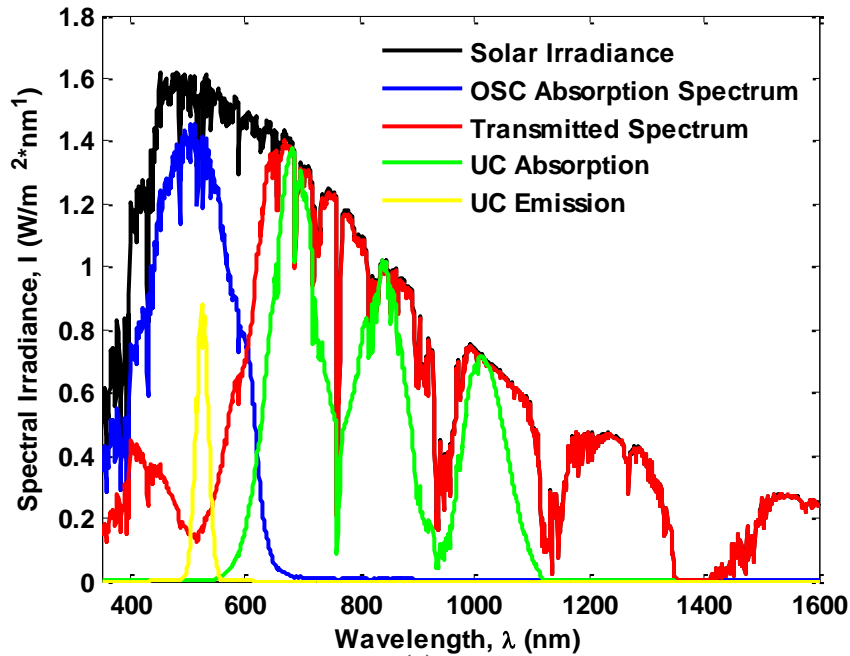
Figure 15: (a) Spectral Irradiance of absorption of and transmission of 200 nm thick P3HT:PCBM based structure S3. (b) Corresponding absorption in UC layer of S3. (c) Emission from three sensitizer based UC layer of S3 at 20% upconveter efficiency along with other spectra for three sensitizer based UC layer.

Figure 16 shows the plot of PCE and upconverted current density with respect to the upconverter efficiency for one, two and three sensitizers based UC system. As seen from figure 16, both the

efficiency for one, two and three sensitizers based UC system. As seen from figure 16, both the

upconverted short circuit current and PCE increases with increasing efficiency. This is obvious, since highly efficient upconverter layer will be able to emit more smaller wavelengths and thus improving power absorption. It is also noteworthy that, more sensitizer molecule based upconverter system yields more PCE and upconverted short circuit current density than fewer sensitizer based system. This is also understandable since, two sensitizer molecules with complementary absorption profiles will absorb more unused power in total than one sensitizer molecule. The total power absorbed by one, two and three sensitizer based system has been found to be 12.9 mW/cm^2, 22.9 mW/cm^2 and 29.7 mW/cm^2 respectively. For one sensitizer based system, the PCE at 50% UC efficiency (theoritical limit for TPA) falls below 4.55% (maximum PCE of non-trasnparent cell). However, for two and three sensitizer based UC layer, PCE exceeds the benchmark of 4.55%. The maximum PCE has been noted as 5.95% which has been obtained for three sensitizer based system with efficiency 50%. This denotes a possible 30.77% enhancement in PCE from conventional structure.

Figure 16: Variation of (a) PCE and (b) Upconverted current density with upconverter efficiency for one (blue), two (green) and three (red) sensitizer-based UC layer in P3HT:PCBM based S3 structure. The parameter *i* in the inset indicates the number of sensitizer molecules in UC layer. The blue, green and red circled markers represent simulation points. The solid lines do not refer to results rather provides a guide to eye.

3.2.2 PSBTBT:PCBM Based OSC

Similar to analysis and discussion in 3.2.1, variation of PCE and other FOM parameters with thickness for PSBTBT:PCBM based S1 and S3 structures has been manifested in figure 17. For conventional structure, the highest efficiency has been noted at 80 nm thickness where PCE reaches up to 5.02% with J_{SC} = 12.92 mA/cm^2, V_{OC} = 0.689 V and FF = 56.34%. For transparent cell, highest PCE has been noted at a lower thickness of 60 nm where For conventional structure, the highest efficiency has been noted at 80 nm thickness where PCE reaches up to 3.74% with J_{SC} = 9.85 mA/cm^2, V_{OC} = 0.688 V and FF = 55.06%. Dominant bimolecular recombination process is the main cause of sharp decay in PCE with increasing thickness for PSBTBT:PCBM. This is why maximum PCEs' have been observed at low thicknesses for both transparent and conventional structures. The transparent cell with 60 nm active layer thickness absorbs 27.7 mW/cm^2 optical power and rejects the rest. This implies approximately 70 mW/cm^2 optical power is available for upconversion. This is done by placing a UC layer with three different sensitizer-annihilator/activator molecules having optimum position of peak absorbance and emittance (listed in Table 6).

With optimzed UC layer, PCE and upconverted current density for one, two and three optimized sensitizer molecule based UC layer have been plotted against the upconverter quantum efficiency. At 50% quantum efficiency, PCE of 4.89%, 5.63% and 6.24% has been observed for one, two and three sensitizer-based molecule system respectively with upconverted current density reaching up to 6.58 mA/cm^2 for three sensitizer-based system. Comparing with the value obtained for conventional structure, the PCE enhancement for this material has been estimated up to 24.3%. The optical powers absorbed by one, two and three sensitizer based UC layer has been calculated as 12.32, 20.96 and 27.74 mW/cm^2 respectively.

Figure 17: Variation of (a) Power Conversion Efficiency (PCE) (b) Short Circuit Current Density (c) Open Circuit Voltage and (d) Fill Factor with active layer thickness for conventional (S1) and transparent structures (S3) of PSBTBT:PCBM based OSC. The blue and red circled markers represent simulation points. The solid lines do not refer to results rather provides a guide to eye.

Table 6: Optimized parameters of absorber and emitter molecules spectral characteristics for 60 nm thick PSBTBT:PCBM based S3 structure.

Molecule	Peak Position (nm)			FWHM (nm)
Sensitizer (Absorber)	606	861	1017	100
Annihilator (Emitter)	520			25
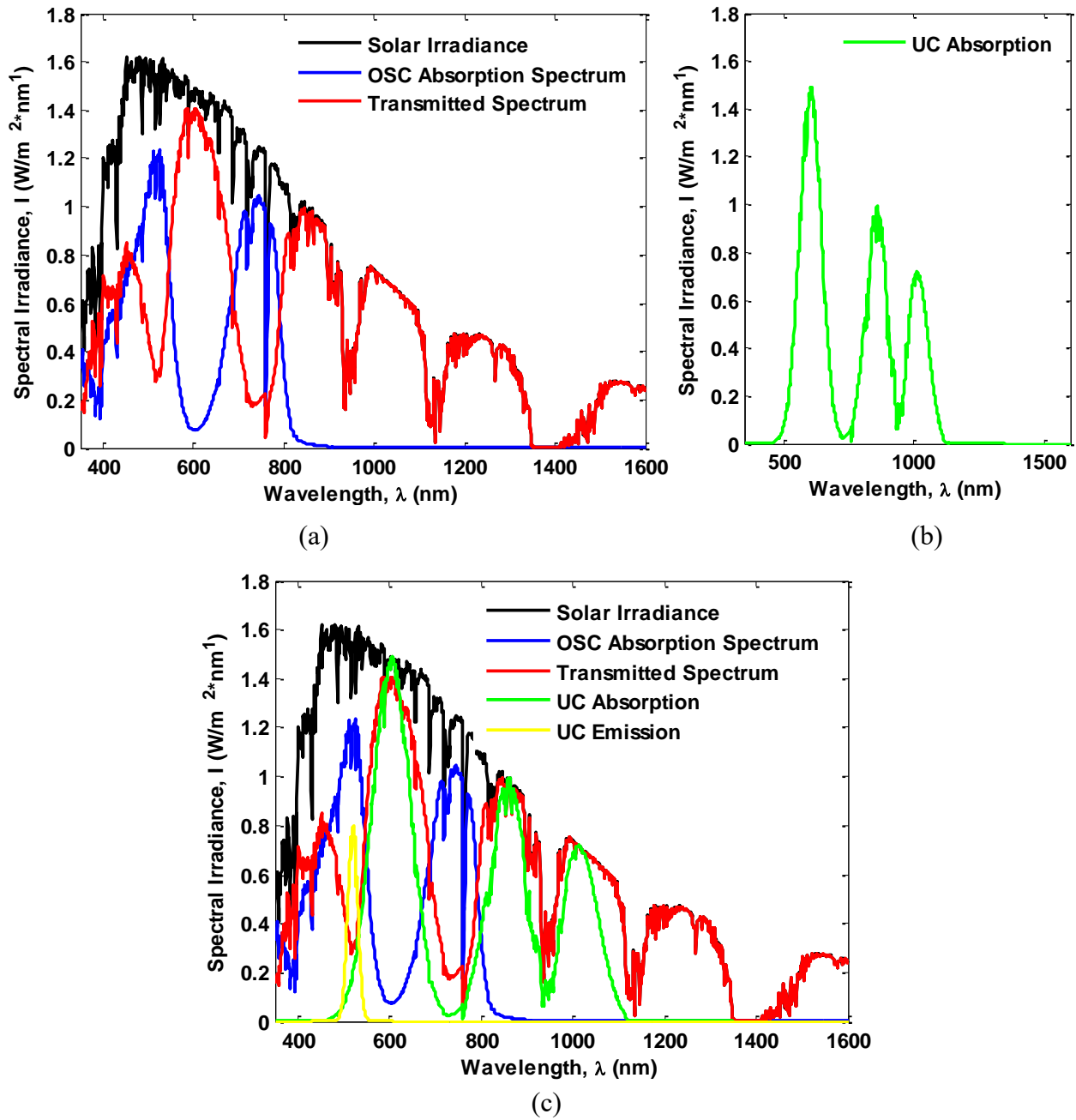
Figure 18: (a) Spectral Irradiance of absorption of and transmission of 60 nm thick PSBTBT:PCBM based structure S3. (b) Corresponding absorption in UC layer of S3. (c) Emission from three sensitizer based UC layer of S3 at 20% upconveter efficiency along with other spectra for three sensitizer based UC layer.
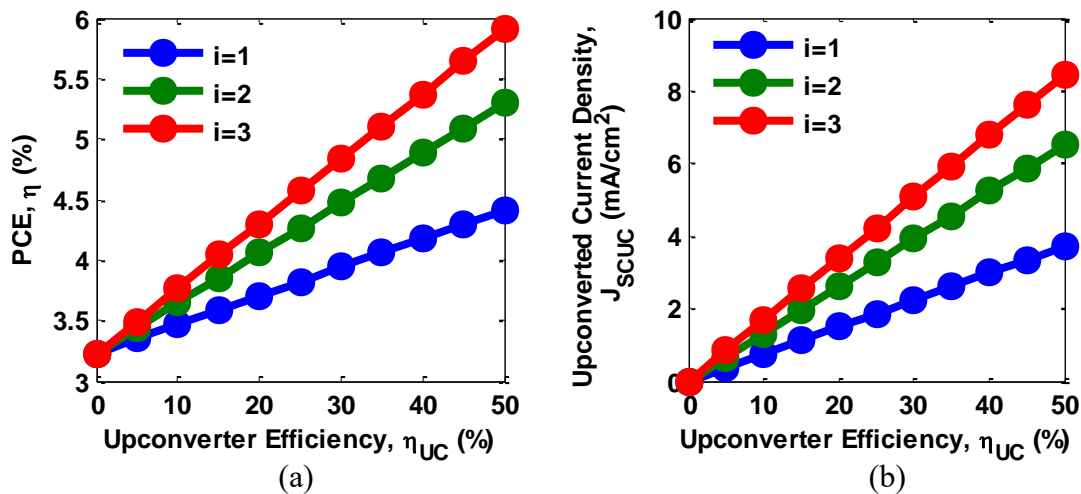
Figure 19: Variation of (a) PCE and (b) Upconverted current density with upconverter efficiency for one (blue), two (green) and three (red) sensitizer-based UC layer in PSBTBT:PCBM based S3 structure. The parameter i in the inset indicates the number of sensitizer molecules in UC layer. The blue, green and red circled markers represent simulation points. The solid lines do not refer to results rather provides a guide to eye.

3.2.3 PBDTTT-C:PCBM Based OSC

For PBDTTT-C:PCBM, both S1 and S3 structures yield maximum PCE at 100 nm with values being 6.35% and 5.30% respectively. The transparent cell absorbs 39.4 mW/cm^2 solar power while transmitting 60 mW/cm^2 to the UC layer. With optimized sensitizer molecule absorption and emission profiles (listed in Table 7), 9.72, 16.38 and 25.53 mW/cm^2 solar power has been harvested by one, two and three sensitizer-based UC layer respectively. With 50% efficient layer, a PCE enhancement of 28.97% was obtained for three sensitizer-based UC layer (PCE= 8.19%). A total 6.28 mA/cm^2 current density was upconverted in the process.

(a)   (b)

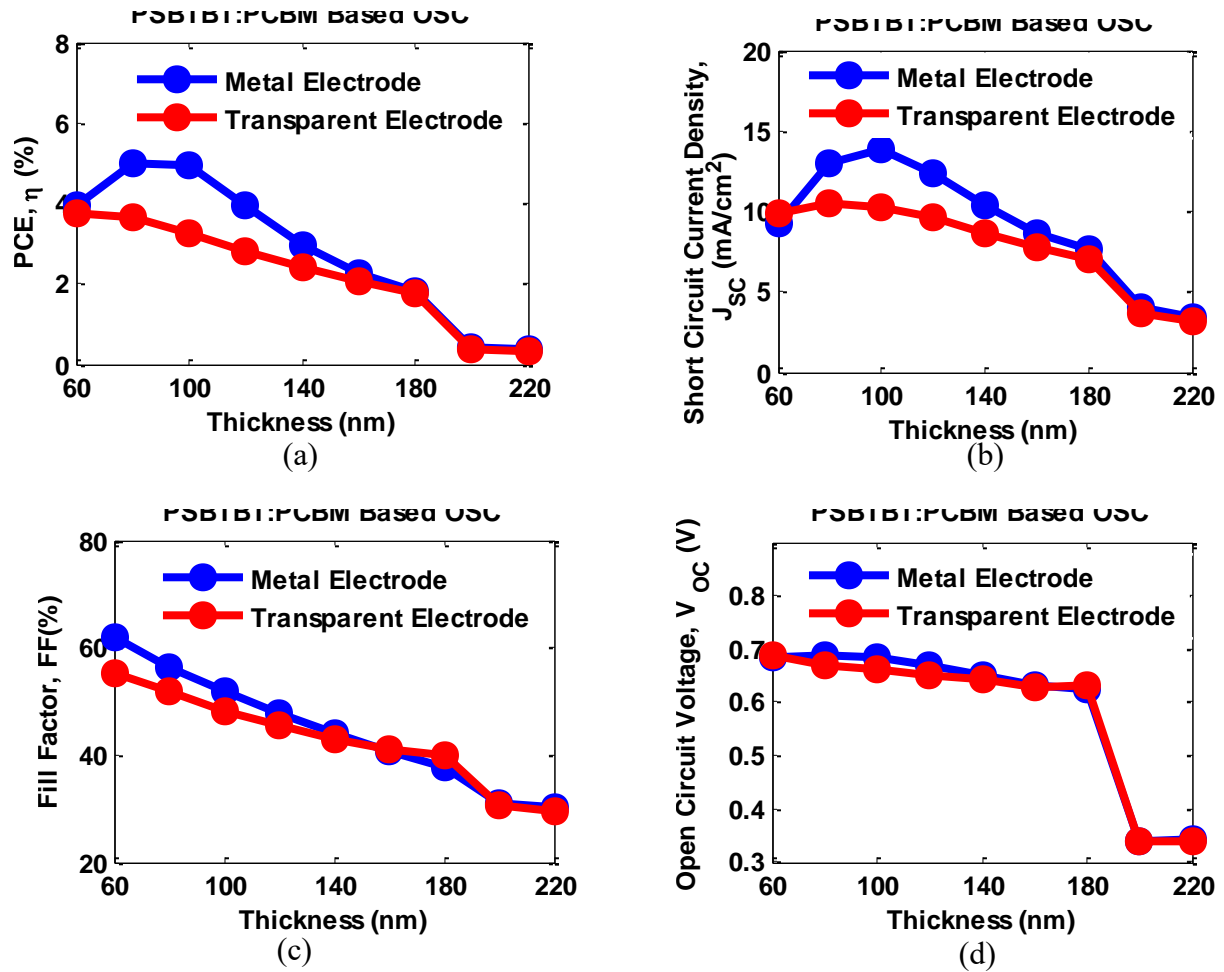(c)   (d)

Figure 20: Variation of (a) Power Conversion Efficiency (PCE) (b) Short Circuit Current Density (c) Open Circuit Voltage and (d) Fill Factor with active layer thickness for conventional (S1) and transparent structures (S3) of PBDTTT-C:PCBM based OSC. The blue and red circled markers represent simulation points. The solid lines do not refer to results rather provides a guide to eye.

Table 7: Optimized parameters of absorber and emitter molecules spectral characteristics for 100 nm thick PBDTTT-C:PCBM based S3 structure.

| Molecule	Peak Position (nm)			FWHM (nm)
Sensitizer (Absorber)	823	1028	1251	100
Annihilator (Emitter)	677			25
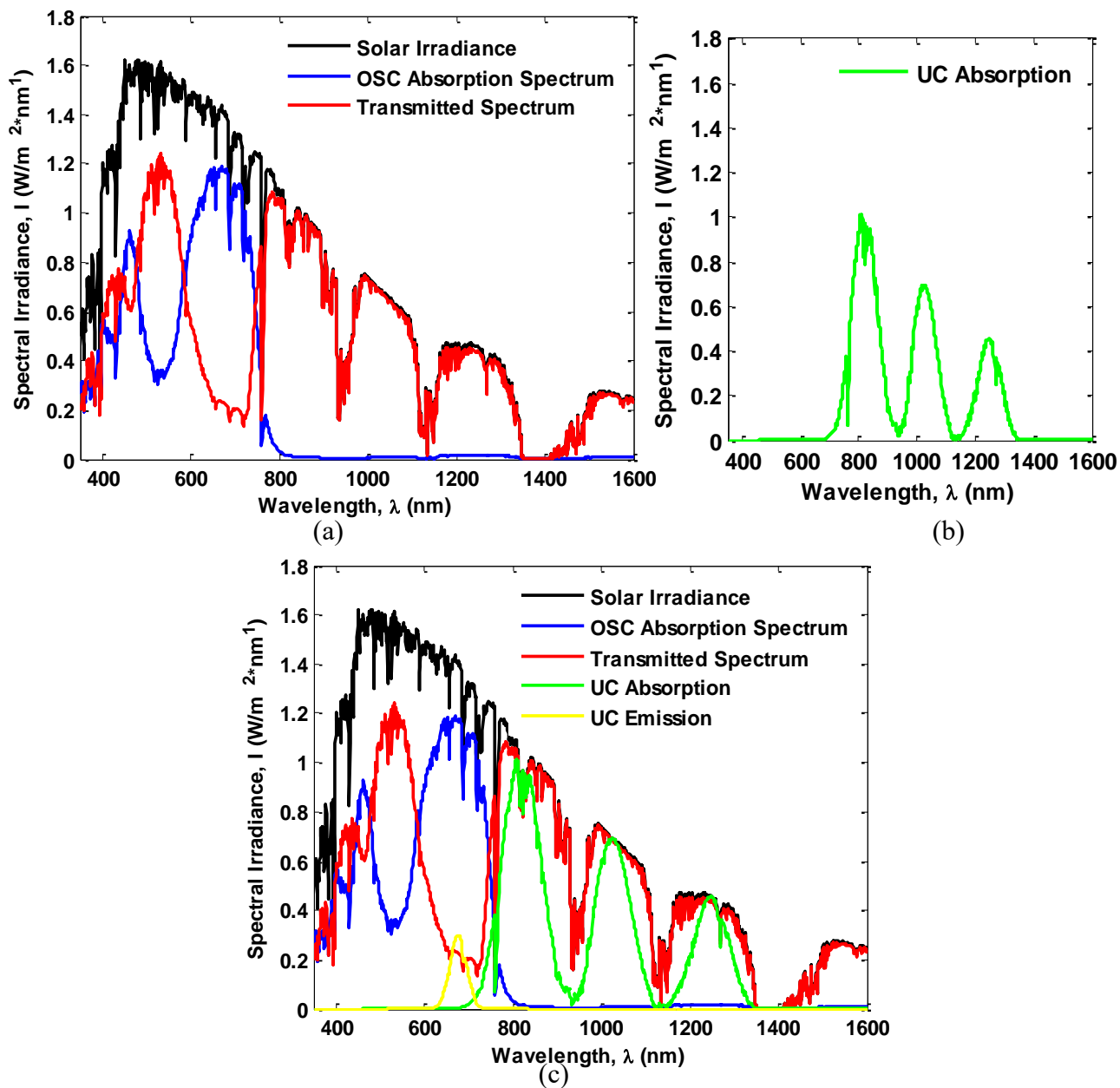
Figure 21: (a) Spectral Irradiance of absorption of and transmission of 100 nm thick PBDTTT-C:PCBM based structure S3. (b) Corresponding absorption in UC layer of S3. (c) Emission from three sensitizer based UC layer of S3 at 20% upconveter efficiency along with other spectra.
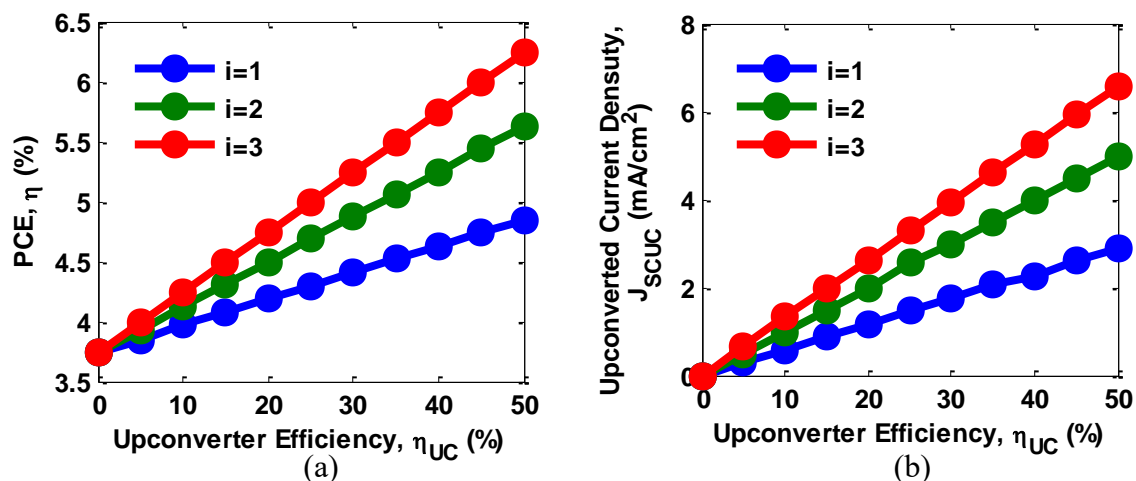
Figure 22: Variation of (a) PCE and (b) Upconverted current density with upconverter efficiency for one (blue), two (green) and three (red) sensitizer-based UC layer in 100 nm PBDTTT-C:PCBM based S3 structure. The parameter i in the inset indicates the number of sensitizer molecules in UC layer. The blue, green and red circled markers represent simulation points. The solid lines do not refer to results rather provides a guide to eye.

3.2.4 PTB7-Th:PCBM Based OSC

The final material that has been chosen to study the effect of upconversion is PTB7-Th:PCBM. An inverted structure (S2) of PTB7-Th:PCBM based OSC has been modelled in this regard. The highest PCE obtained for the inverted structure is 10.55% with J_{SC} = 19.06 mA/cm^2, V_{OC} = 0.7683 V and FF = 72.07% at 80 nm active layer thickness. For S4 structure with PTB7-Th:PCBM, highest PCE has been noted at 120 nm where where PCE reaches up to 8.82% with J_{SC} = 18.01 mA/cm^2, V_{OC} = 0.76 V and FF = 64.85%. The cell absorbs 51 mW/cm^2 solar power (up to 750 nm wavelengths) and after minute loss in trasnparent electrode, approximately 48 mW/cm^2 solar power is available for upconversion. In this regard, the spectral cahracterisitcs of upconverting molecules have been optimized and listed in table 8. Similar to other materials, the PCE and upconverted current density have been plotted against upconverter efficiency for optimized one, two and three sensitizer-based UC layer. At 50% efficiency, PCE of 10.43%, 11.59% and 12.34%

(a maximum 17% enhancement) respectively have been noted for one, two and three sensitizer-based UC layer. The optical power absorbed by the one, two and three sensitizer-based UC layer has been found to be 9.36 mW/cm^2, 16.1 mW/cm^2 and 20.43 mW/cm^2.
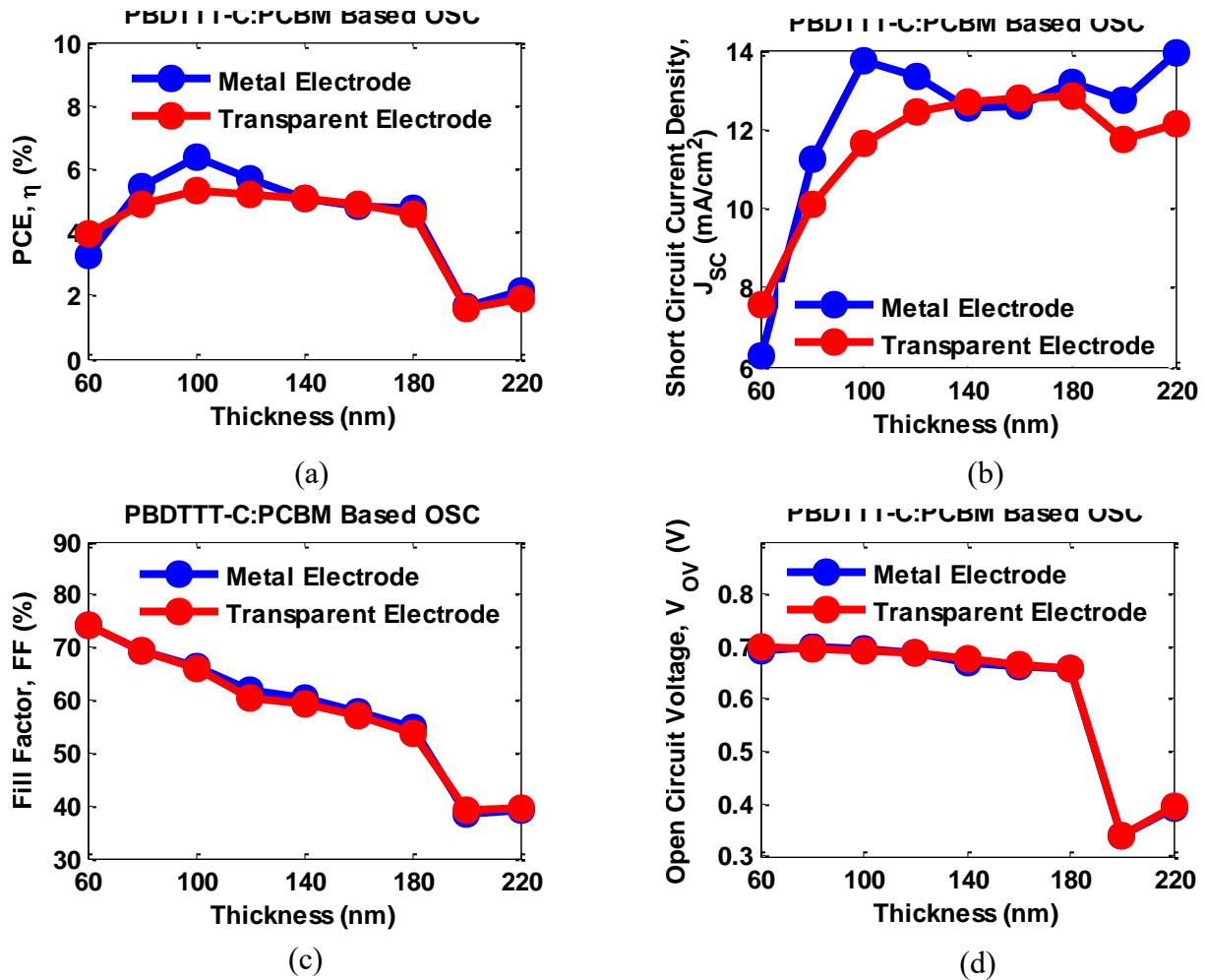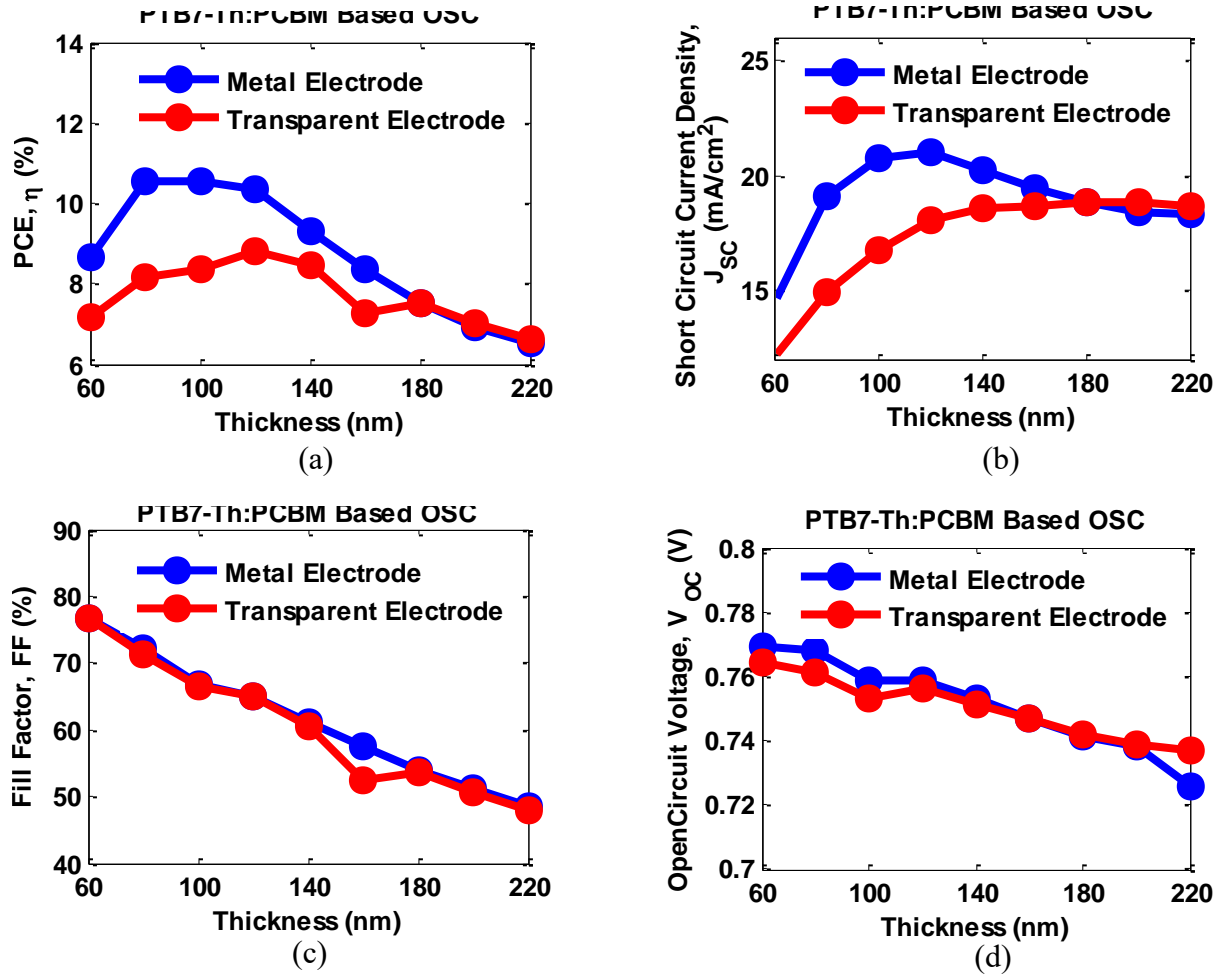

Figure 23: Variation of (a) Power Conversion Efficiency (PCE) (b) Short Circuit Current Density (c) Open Circuit Voltage and (d) Fill Factor with active layer thickness for inverted (S2) and transparent structures (S4) of 120 nm PTB7-Th:PCBM based OSC. The blue an and red circled markers represent simulation points. The solid lines do not refer to results rather provides a guide to eye.

Table 8: Optimized parameters of absorber and emitter molecules spectral characteristics for 120 nm thick PTB7-Th:PCBM based S3 structure.

| Molecule	Peak Position (nm)			FWHM (nm)
Sensitizer (Absorber)	817	1017	1240	100
Annihilator (Emitter)	669			25
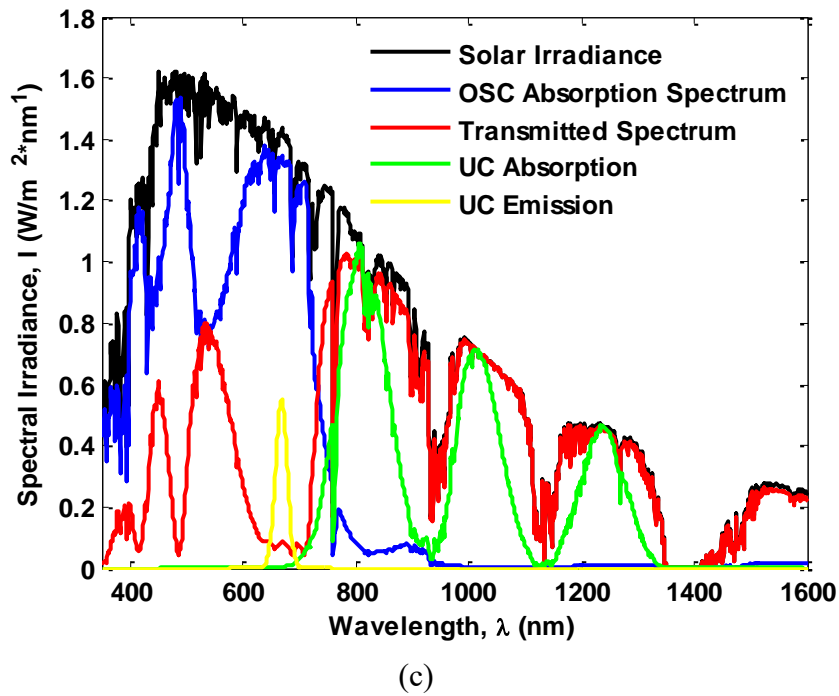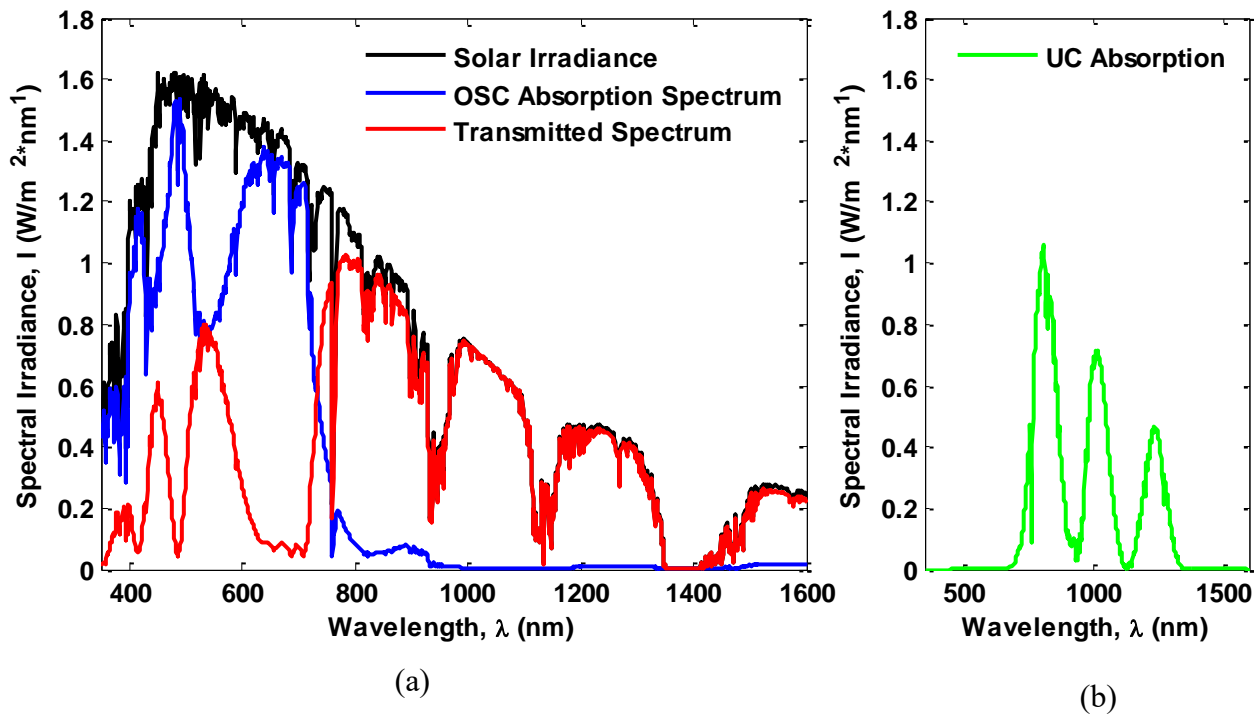
Figure 24: (a) Spectral Irradiance of absorption of and transmission of 120 nm thick PTB7-Th:PCBM based structure S3. (b) Corresponding absorption in UC layer of S3. (c) Emission from three sensitizer-based UC layer of S3 at 20% upconveter efficiency along with other spectra.
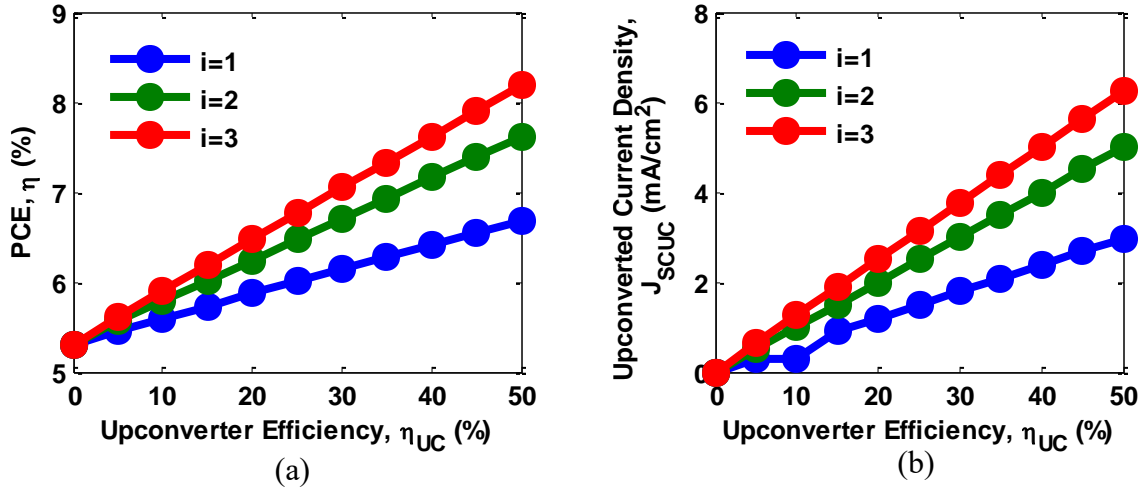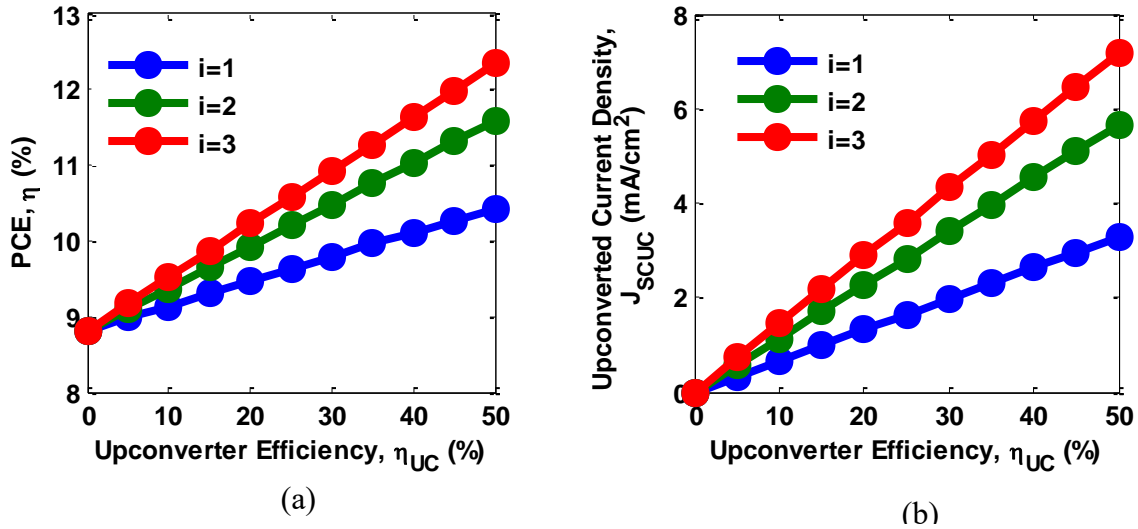
Figure 25: Variation of (a) PCE and (b) Upconverted current density with upconverter efficiency for one (blue), two (green) and three (red) sensitizer-based UC layer in 80 nm PTB7-Th:PCBM based S4 structure. The parameter *i* in the inset indicates the number of sensitizer molecules in UC layer. The blue, green and red circled markers represent simulation points. The solid lines do not refer to results rather provides a guide to eye.

3.3 Effect of Metallic Nanoparticles (Plasmonic Effect)

After demonstrating the effect of upconversion process on OSC, the focus of the thesis has been shifted into demonstrating the effect of metallic nanoparticles (MNPs) in PCE enhancement of OSCs. For OSCs, this effect has been previously reported by many researchers over the years. However, effect of MNPs in PCE enhancement of PTB7-Th:PCBM has not been reported. Moreover, to meet thesis objective four, it is necessary to study the effect of both upcovnersion and MNP insertion to arrive at highly efficient OSC. The most efficient OSC is, of course, PTB7-Th:PCBM, as manifested from section 3.2.4, with or without upconversion process. So, in this section the effect of inserting MNPs only in PTB7-Th:PCBM based OSCs' has been summarized.

For efficiency enhancement, silver nanowires (SNW) have been placed inside active layer. Then the height and the width of the SNWs' have been optimized. FOR SNW height and width of 60

and 80 nm respectively the efficiency is maximized. A possible 13.5% enhancement has been

noted at this configuration of SNW with PCE reaching up to 11.97% with $J_{SC} = 21.58$ mA/cm^2,

$V_{OC} = 0.773$ V and FF = 71.79% for 80 nm active layer thickness.
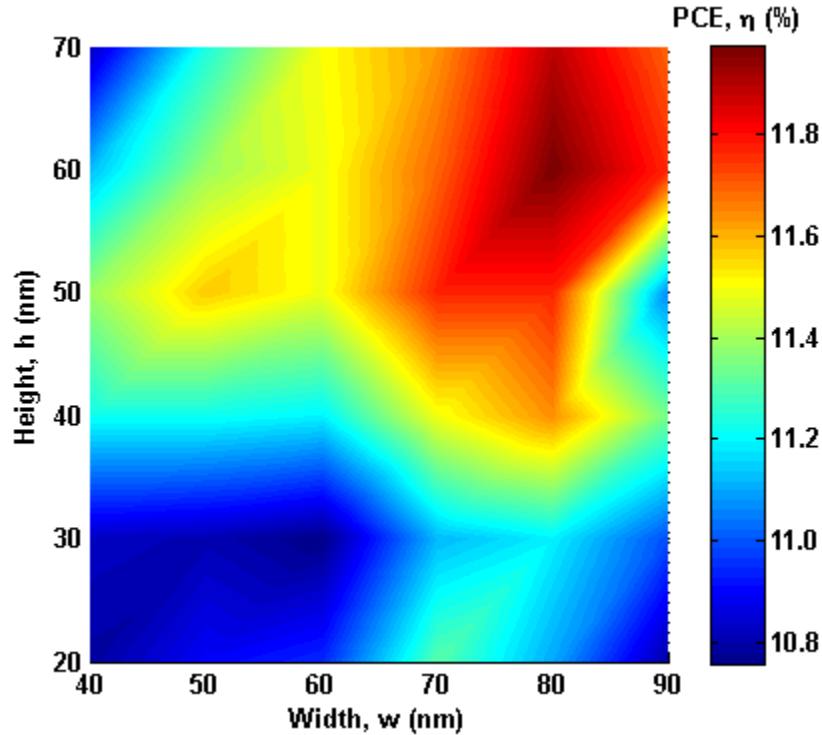
Figure 26: 2D surface plot of PCE with varying width (x axis) and height (y axis) of silver
nanowires placed 420 nm apart each other in 80 nm thick PTB7-Th:PCBM based OSC. The plot
is obtained by interpolating 49 simulation points (w,h) as marked by the ticks in both axis.

The PCE enhancement at the optimized dimension has been investigated by initially comparing

the power absorbtion profiles of the optimized and unaided structures having 3 nm mesh. From

figure 27 (a) and (b), it is obvious that, the power absorption increases significantly from unaided

to optimized structure. To be precise, two sharp peaks have been observed in the power absorption

profiles in optimized structures which are mainly responsible for significant short circuit current

density increase. The integrated power absorptions have been calculated as 37.45% and 43.66%

for unaided and optimized structure respectively.
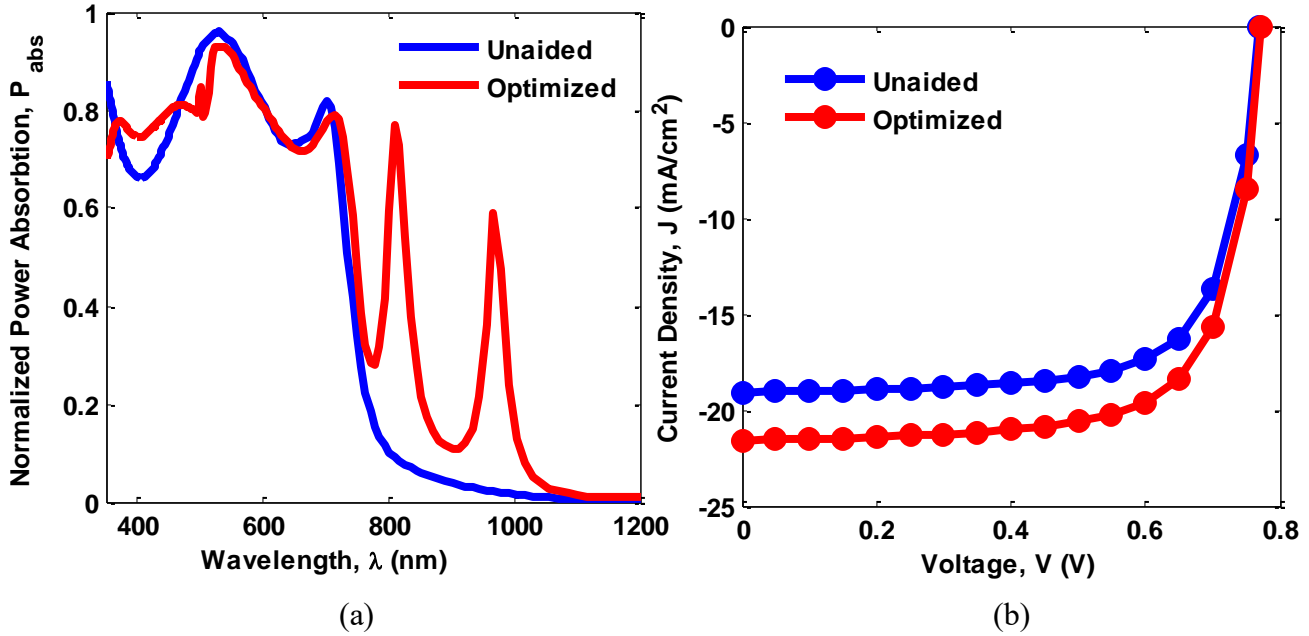
Figure 27: Comparison of (a) power absorption profiles and (b) JV characteristics of unaided and SNW optimized structures. The blue and red circled markers represent simulation results. The solid lines do not represent results rather provides a guide to eye.
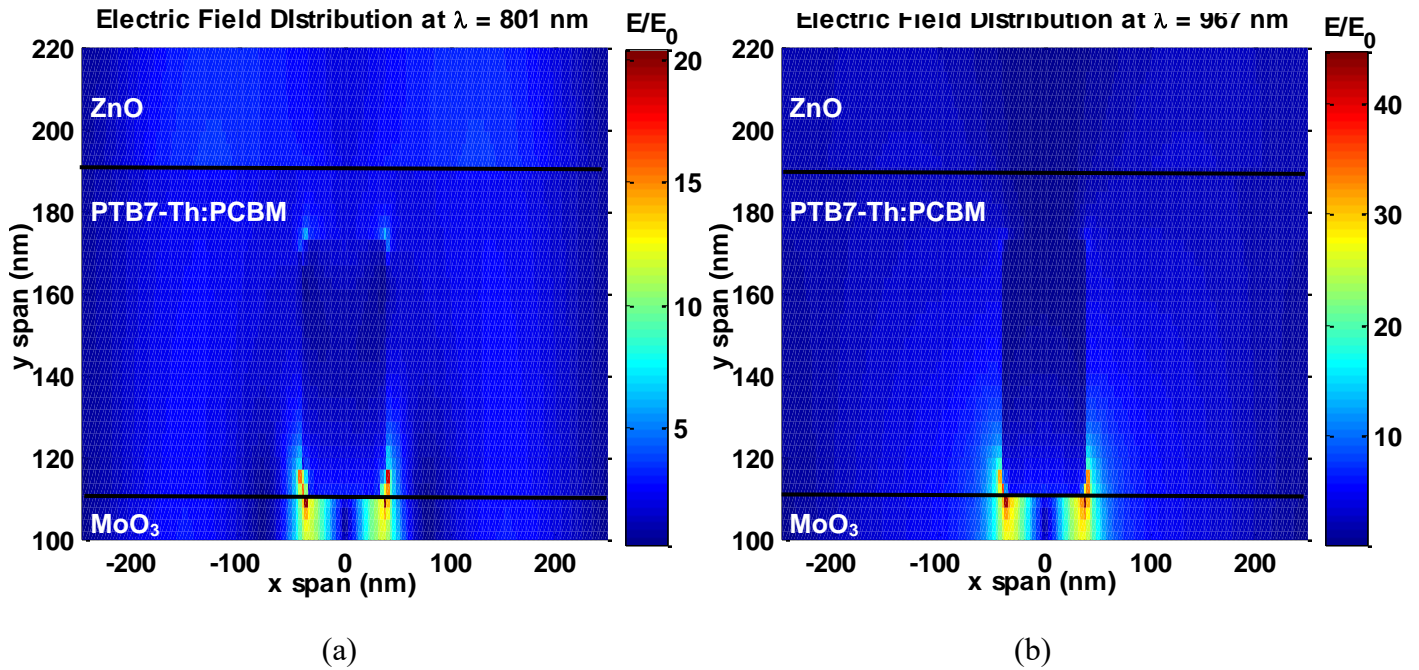
Figure 28: Optical electric field distribution inside the active layer for optimized SNW at (a) 801 nm and (b) 967 nm wavelengths. The colour bars indicate the optical electric field enhancement whereas the black lines indicate the interface between different layers.

For further investigation, the optical electric field intensity has been investigated for the optimized structures at wavelengths 801 nm and 966 nm where sharp peaks have been observed in the structures' power absorption profile. In the optical electric field distribution, high electric field enhancements (nearly 43 times at 967 nm wavelength) have been observed at metal/dielectric interface which attribute to enhanced power absorptions at both 801 nm (Figure 28 (a)) and 967 nm (Figure 28 (b)) wavelengths.

3.4 Effect of Upconversion and Metallic Nanoparticles Combined

In section 3.2.4, it has been demonstrated that a possible 17% PCE enhancement is possible (from 10.55%) for PTB7-Th:PCBM based OSC by three sensitizer molecule based upconverter layer with PCE = 12.34%. In section 3.3, it has also been estimated that, for the same OSC, a 13.45% enhancement with PCE= 11.97% is possible with optimized silver nanowire. Of course, it is intimidating to study the combined effect of upconversion and nanostructures on the most efficient OSC i.e. PTB7-Th:PCBM.

In this regard, the optimized structure from section 3.3 has been taken into account and the metal electrode has been replaced by ZnO:Al and corresponding S4 structure has been developed. The modified structures PCE decreases significantly where the structure loses 4.5 mA/cm^2 current density. This is mainly because in S4 configuration of the optimized structure, the plasmonic resonance vanishes at 801 nm and 967 nm and the overall optical electric field enhancement is very low (5 times) compared to that of the optimized structure. The PCE of the s4 configuration of optimized structure has been noted as 9.33% with J_{SC} = 16.98 mA/cm^2, V_{OC} = 0.764 V and FF = 72.15%. At this stage, simulations have been carried out for one, two and three sensitizer molecule based UC layer where it has been found that the maximum efficiency that can be obtained

is 12.62% where upconverted light contributes to 5.96 mA/cm^2. This denotes a mere 5% increase in PCE from optimized nanostructured configuration.
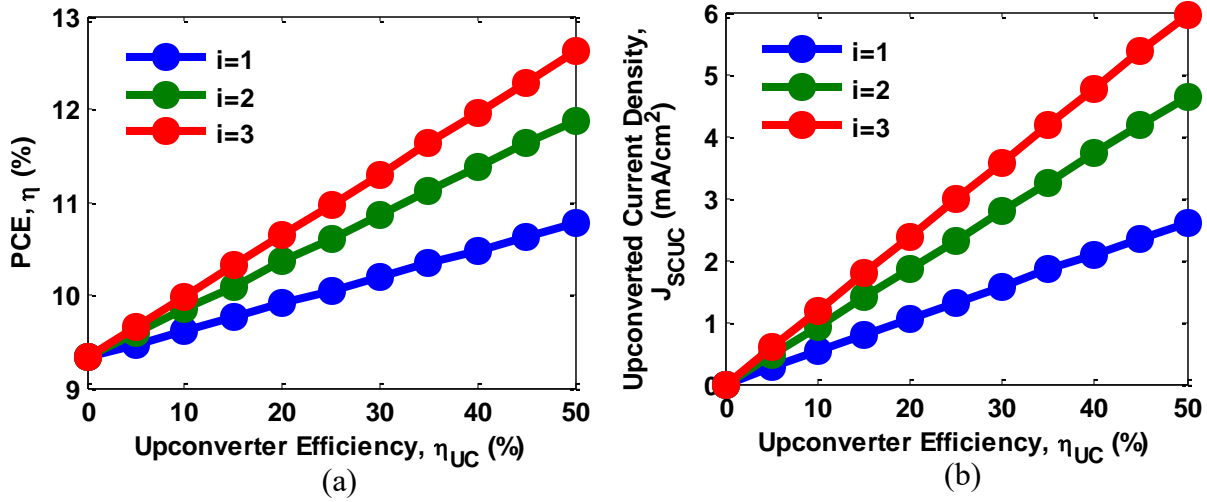
Figure 29: Variation of (a) PCE and (b) Upconverted current density with upconverter efficiency for one (blue), two (green) and three (red) sensitizer-based UC layer in 80 nm PTB7-Th:PCBM based S4 structure with optimized silver nanowire. The parameter i in the inset indicates the number of sensitizer molecules in UC layer. The blue, green and red circled markers represent simulation points. The solid lines do not refer to results rather provides a guide to eye.

3.5 Effect of Concentrated Sunlight on Upconverter Solar Cell

To further improve the PCE of nanostructured solar cell with UC layer, concentrated sunlight has been used. This has been done mainly because, with concentrated sunlight, more sunlight will be available for upconversion. This is also true for solar cell with only UC layer having no nano-plasmonic structure in active layer. It has also been reported in literature that, with concentrated sunlight, upconverter efficiency increases [54]. In this regard, the most efficient solar cell structure developed till section 3.4, has been selected to study the effect of concentrated sunlight on the cell performance. For conservative and practical estimation, from here and what follows, a UC layer

with two (i=2) sensitizer molecules having 15% upconverting efficiency has been selected for studying the effect.

Using the methodology described in section 2.3.5, concentrated sunlight has been incorporated in the opto-electronic simulation environment and multiple simulations have been carried away for different sunlight concentrations ranging from 1 to 10. Due to stability and degradation issue, sunlight with higher concentrations have been discarded. Even at 10 sun illumination, organic photovoltaic cell degradation is a concern [68]. However, to predict the behavior at ideal conditions, up to 10 sun illuminations have been considered. Practical solar cells with concentrated sunlight may underperform than predicted.
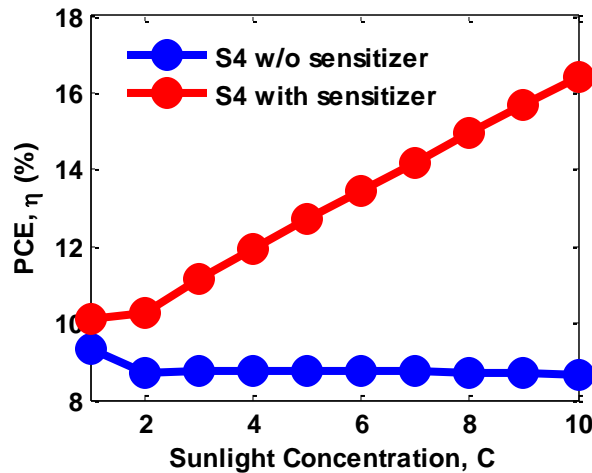
Figure 30: Variation of PCE of nanostructure incorporated PTB7-Th:PCBM based OSC having S4 structure with and without upconverting molecules at different sunlight concentration. The upconverter layer is assumed to have two sensitizer molecules with the efficiency of the system being 15%. The blue and red circled markers in the plot represent simulation points. The solid lines do not refer to results rather provide a guide to eye.

Figure 30 shows the variation of PCE with varying solar concentration. From the study, it has been observed that, the PCE of nanostructure incorporated PTB7-Th:PCBM based OSC decreases slowly with increasing sunlight concentrations. The PCE at 10 sun illuminations for this OSC has

been noted as 8.61% whereas PCE of 1 sun illumination was 9.33%. With upconverting molecules, the PCE increases with increasing concentration. This is understandable, since more optical power is available for upconversion for concentrated sun light. It has been predicted from the study that, two sensitizer molecules based UC layer with 15% upconversion efficiency, if placed with nanostructure incorporated S4 structure, will yield a 16.4% PCE under 10 sun illumination.

Chapter 4

Conclusion and Future Work

4.1 Conclusions

In this thesis, an FDTD model to study the effect of upconversion in solar cell has been developed. Then, using the model, we have studied the effect of upconversion process on four different organic solar cells (OSC) having different structures and active materials. In each case, the upconverter behavior has been optimized to harness maximum optical power possible and deliver most of the absorbed power at a wavelength where to absorption of the active material is highest. Then, we have predicted the power conversion efficiency (PCE) of the OSCs for different upconverter efficiency. As a separate study, metallic nanowires (MNW) have been placed inside the most efficient OSC to observe the variation of PCE with varying dimensions of the MNW. From the study an optimum OSC structure with optimized MNW dimension has been obtained. Results obtained from the separate studies have been combined to estimate PCE. Then concentrated sunlight has been used to enhance PCE furthermore. In conclusion, the major observations and contributions of this works are as follows:

- A detailed FDTD model of photonic upconversion for solar cell was developed to predict the effect of upconverting materials on P3HT:PCBM, PSBTBT:PCBM, PBDTTT-C:PCBM and PTB7-Th:PCBM based organic solar cell performances having optimized spectral parameters and different efficiencies.

- Upconverter spectral characteristics was optimized for four different active material based organic solar cell and up to 30% enhancement in PCE has been recorded from unaided structures for P3HT:PCBM based OSC. For PSBTBT:PCBM, PBDTTT-C:PCBM and PTB7-Th:PCBM, the enhancements were 25%, 29% and 17% respectively. Although P3HT:PCBM based OSC has better enhancement, the maximum PCE has been observed in case of PTB7-Th:PCBM.

- Plasmonic effect on PTB7-Th:PCBM based OSC has been studied by placing an optimized silver nanowire and nearly 14% enhancement in efficiency has been observed from unaided structure.

- Combined effect of upconversion and MNW has also been studied and nearly 5% enhancement from individual effect has been noted.

- Concentrated sunlight has been used to predict the PCE of OSC at many sun illuminations and for a practical 15% upconverter efficiency and with optimized MNW, it has been found that PCE of nearly 16.5% is achievable for 10 sun illumination. This denotes a 50% enhancement from the unaided structures' efficiency which is 10.55%

It is expected that, the observations and contributions made in this scope will provide a comprehensive understanding in related topics and inspire fabrication of most efficient structure.

4.2 Future Works

As mentioned in chapter 2, the model developed in this work is capable of handling upconverter layer emitting only one wavelength. Practical upconverter layers can emit multiple wavelengths and thereby providing more optical power to the active material. So, a possible extension of this work would be to improve and modify the model for multi-emission spectra. The techniques used to enhance PCE of OSC in this thesis mainly focuses on enhancing optical power absorption. Focusing on both optical power absorption enhancement and improved charge transportation system was beyond the scope of this work. So, an obvious future work of the scope will be to focus on improved charge transportation system of the most efficient material to enhance the PCE furthermore.

References

[1] "United Nations," [Online]. Available: https://www.un.org/sustainabledevelopment/sustainable-development-goals/. [Accessed 15 September 2018].

[2] T. M. Razykov, C.S.Ferekides, D.Morel, E.Stefanakos, H.S.Ullal and H.M.Upadhyaya, "Solar photovoltaic electricity: Current status and future prospects," *Solar Energy,* vol. 85, no. 8, pp. 1580-1608, 2011.

[3] R. Nault, "Report on the basic energy sciences workshop on solar energy utilization," Agronne National Laboratory USA, 2005.

[4] K.H. Solangi, M.R.Islam, R.Saidura, N.A.Rahim and H.Fayaz, "A review on global solar energy policy," *Renew. Sustain. Energy Rev.,* vol. 15, no. 4, pp. 2149-2163, 2011.

[5] S. Sharma, K. K. Jain and A. Sharma, "Solar Cells: In Research and Applications—A Review," *Mater. Sci. Appl.,* vol. 6, no. 12, pp. 1145-1155, 2015.

[6] T. Ibn. Mohammed , S.C.L.Koh, I.M.Reaney , A.Acquaye, G.Schile, K.B.Mustapha and R.Greenough, "Perovskite solar cells: An integrated hybrid lifecycle assessment and review in comparison with other photovoltaic technologies," *Renew. Sustain Energy Rev,* vol. 80, pp. 1321-1344, 2017.

[7] "National Renewable Energy Laboratory," [Online]. Available: https://www.nrel.gov/pv/assets/images/efficiency-chart-20180716.jpg. [Accessed 15 September 2018].

[8] F. Krebs, "Fabrication and processing of polymer solar cells: A review of printing and coating techniques," *SOLMAT,* vol. 93, no. 4, pp. 394-412, 2009.

[9] B. Kippelen and J.-L. Bredus, "Organic photovoltaics," *Energy Environ. Sci.,* vol. 2, pp. 251-261, 2009.

[10] G. Li., L. Liu, F. Wei, S. Xia and X. Qian, "Recent Progress in Modeling, Simulation, and Optimization of Polymer Solar Cells," *IEEE Journal of Photovoltaics,* vol. 2, no. 3, pp. 320-340, 2012.

[11] S. H. Park, A. Roy, S. Beaupré, S. Cho, N. Coates, J. S. Moon, D. Moses, M. Leclerc, K. Lee & A. J. Heeger, "Bulk heterojunction solar cells with internal quantum efficiency approaching 100%," *N. Photon.,* vol. 3, pp. 297-302, 2009.

[12] R. Hausermann, E. Knapp, M. Moos, N. A. Reinke, T. Flatz, and B. Ruhstaller, "Coupled optoelectronic simulation of organic bulk-heterojunction solar cells: Parameter extraction and sensitivity analysis," *J. Appl. Phys.,* vol. 106, p. 104507, 2009.

[13] A. Bagher, "Comparison of organic solar cells and inorganic solar cells," *Intl J. Renew. and Sustain. Energy,* vol. 3, no. 3, pp. 53-58, 2014.

[14] F. Krebs, "All solution roll-to-roll processed polymer solar cells free from indium-tin-oxide and vaccum coating steps," *Org. Electron. ,* vol. 10, no. 5, pp. 761-768, 2009.

[15] A Singh, A. Dey, D. Das and P. K. Iyer, ""Combined Influence of Plasmonic Metal Nanoparticle and Dual Cathode Buffer Layer for Highly Efficient rrP3HT: PCBM Based Bulk Heterojunction Solar Cell," *J. Mater. Chem. C,* vol. 5, no. 26, pp. 6578-6587, 2017.

[16] K. N'konou, L. Peres and P. Torchio, "Optical Absorption Modeling of Plasmonic Organic Solar Cells Embedding Silica coated Silver Nanospheres," *Plasmonics ,* vol. 13, no. 1, pp. 297-303, 2018.

[17] M. L. Tsai, Meng-Lin Tsai, Wan-Rou Wei†, L. Tang, Hung-Chih Chang, Shih-Hsiang Tai, Po-Kang Yang, Shu Ping Lau, Lih-Juann Chen, and Jr-Hau He, "Si Hybrid Solar Cells with 13% Efficiency via Concurrent Improvement in Optical and Electrical Properties by Employing Graphene Quantum Dots," *ACS Nano,* vol. 10, no. 1, pp. 815-821, 2015.

[18] S. H. Tsai, "Toward high efficiency of inverted organic solar cells: Concurrent improvement in optical and electrical properties of electron transport layers," *Appl. Phys. Lett.,* vol. 102, p. 253111, 2013.

[19] J. Nelson, "Polymer:fullerene bulk heterojunction solar cells," *Mater. Today,* vol. 14, no. 10, pp. 462-470, 2011.

[20] C. W. Tang, "Two-layer organic photovoltaic cell," *Appl. Phys. Lett.,* vol. 48, no. 2, p. 183, 1986.

[21] D. E. Markov, E. Amsterdam, Paul W. M. Blom, Alexander B. Sieval, and Jan C. Hummelen., "Accurate Measurement of the Exciton Diffusion Length in a Conjugated Polymer Using a Heterostructure with a Side-Chain Cross-Linked Fullerene Layer," *J. Phys. Chem. A,* vol. 109, no. 24, pp. 5266-5277, 2005.

[22] G. Yu, J. Gao, J. C. Hummelen, F. Wudl, and A. J. Heeger, "Polymer Photovoltaic Cells: Enhanced Efficiencies via a Network of Internal Donor-Acceptor Heterojunctions," *Science ,* vol. 270, no. 5243, pp. 1789-1791, 1995.

[23] M. Granstrom, K. Petritsch, A. C. Arias, A. Lux, M. R. Andersson & R. H. Friend, "Laminated fabrication of polymeric photovoltaic diodes," *Nature,* vol. 395, pp. 257-260, 1998.

[24] H. B. D. Hertel, "Photoconduction in amorphous organic solids.," *Chem. Phys. Chem.,* vol. 9, no. 5, pp. 666-688, 2008.

[25] A. H. Fallahpour, G. Ulisse, M. Auf der Maur, A. Di Carlo and F. Brunetti, "3-D Simulation and Optimization of Organic Solar Cell With Periodic Back Contact Grating Electrode," *IEEE Journal of Photovoltaics,* vol. 5, no. 2, pp. 591-596, 2014.

[26] K. Jung, Hyung-Jun Song, G. Lee, Y. Ko, K. Ahn, H. Choi, J. Y. Kim, K. Ha, J. Song; Jong-K. Lee, C. Lee and M. Choi, "Plasmonic Organic Solar Cells Employing Nanobump Assembly via Aerosol-Derived Nanoparticles," *ACS Nano,* vol. 8, no. 3, pp. 2590-2601, 2014.

[27] A. Shalav, B. S. Richards, and T. Trupke, "Application of NaYF4:Er3+ up-converting phosphors for enhanced near-infrared silicon solar cell response," *Appl. Phys. Lett. ,* vol. 86, p. 013505, 2005.

[28] A. A. D. Adikaari, I. Etchart, Paul-Henri Guéring, M. Bérard, S. Ravi, P. Silva, A. K. Cheetham, and R. J. Curry, "Near infrared up-conversion in organic photovoltaic devices using an efficient Yb3+:Ho3+ Co-doped Ln2BaZnO5 (Ln = Y, Gd) phosphor," *J. Appl. Phys.,* vol. 111, no. 9, p. 094502, 2012.

[29] H. Q. Wang, "Rare-Earth Ion Doped Up-Conversion Materials for Photovoltaic Applications," *Adv. Mater.,* vol. 23, pp. 3675-3680, 2011.

[30] J.L. Wu, "Upconversion effects on the performance of near-infrared laser-driven polymer photovoltaic devices," *Org. Electron.,* vol. 13, pp. 2104-2108, 2012.

[31] Y. Chen, W. He, Y. Jiao, H. Wang, X. Hao, J. Lu and S. Yang , "β-NaYF4:Er3+ (10%) microprisms for the enhancement of a-Si:H solar cell near-infrared responses," *J. Lumin.,* vol. 132, pp. 2247-2250, 2012.

[32] Y. Shang, S. Hao, C. Yang and G. Chen, "Enhancing Solar Cell Efficiency Using Photon Upconversion Materials," *Nanomaterials,* vol. 5, pp. 1782-1809, 2015.

[33] Y. Y. Cheng, B. Fückel, T. Khoury, R. G. C. R. Clady, M. J. Y. Tayebjee, N. J. Ekins-Daukes, M. J. Crossley and T. W. Schmidt., "Kinetic Analysis of Photochemical Upconversion by Triplet-Triplet Annihilation: Beyond Any Spin Statistical Limit," *J. Phys. Chem Lett.,* vol. 1, pp. 1795-1799, 2010.

[34] C. Ye, B. Wang, R. Hao, X. Wang, P. Ding, X. Tao, Z. Chen, Z. Lianga and Y. Zhoua, "Oil-in-water microemulsion: an effective medium for triplet–triplet annihilated upconversion with efficient triplet acceptors," *J. Mater. Chem. C,* vol. 2, no. 40, pp. 8507-8514, 2014.

[35] S. E. Shaheen, C. J. Brabec and N. R. Sariciftci, "2.5% Efficient Organic Plastic Solar Cells," *Appl. Phys. Lett.,* vol. 78, no. 6, p. 841, 2001.

[36] P. Boland, K. Lee and G. Namkoong, "Device optimization in PCPDTBT:PCBM plastic solar cells," *SOLMAT,* vol. 94, no. 5, pp. 915-920, 2010.

[37] M. Zhou, Q. Sun, L. Gao, J. Wu, S. Zhou, Z. Li, Y. Hao and F. Shi, "Enhancement of power conversion efficiency of PTB7:PCBM-based solar cells by gate bias," *Org. Electron.,* vol. 32, no. C, pp. 34-40, 2016.

[38] F. Monestier, Jean-J. Simon, P. Torchio, L. Escoubas, F. Flory, S. Bailly, R. Bettignies, S. Guillerez and C. Defranoux, "Modelling the Short Circuit Current Density of Polymer Solar Cells based on P3HT/PCBM," *SOLMAT,* vol. 91, no. 5, pp. 405-410, 2007.

[39] M. Chowdhury and M. Alam, "An optoelectronic analytical model for bulk heterojunction organic solar cells incorporating position andwavelength dependent carrier generation," *SOLMAT,* vol. 132, pp. 107-117, 2015.

[40] S. Altazin, R. Clerc, R. Gwoziecki, G. Pananakakis, G. Ghibaudo, and C. Serbutoviez, "Analytical modeling of organic solar cells and photodiodes," *Appl. Phys. Lett.,* vol. 99, p. 143301, 2011.

[41] R.C. Coffin, J. Peet, J. Rogers & G. C. Bazan., "Streamlined microwave assisted preparation of narrow-bandgap conjugated polymers for high performance bulk heterojunction solar cells," *N. Chem.,* vol. 1, pp. 657-661, 2009.

[42] P. Morvillo, R. Diana, R. Ricciardi, E. Bobeico and C. Minarini, "High-efficiency standard and inverted polymer solar cells based on PBDTTT-C:[70]PCBM blend," in *IEEE*, Naples, 2017.

[43] T. Kobori and T. Fukuda, "Effect of optical intensity distribution on device performances of PTB7-Th:PC71BM-based organic photovoltaic cells," *Org. Electron.,* vol. 51, pp. 76-85, 2017.

[44] M.S. Islam, "Analytical modeling of organic solar cells including monomolecular recombination and carrier generation calculated by optical transfer matrix method," *Org. Eletron.,* vol. 41, pp. 143-156, 2017.

[45] M. Islam, S. Wahid, M.M. Chowdhury, F. Hakim and M. K. Alam, "Effect of spatial distribution of generation rate on bulk heterojunction organic solar cell performance: A novel semi-analytical approach," *Org. Electron.,* vol. 46, pp. 226-241, 2017.

[46] D. Chi, S. Qu, Z. Wang and J. Wang, "High efficiency P3HT:PCBM solar cells with an inserted PCBM layer," *J. Mater. Chem. C,* vol. 2, pp. 4383-4387, 2014.

[47] X.H. Li, W. E.I. Sha, W. C.H. Choy, D. D. S. Fung, and F. X. Xie., "Efficient Inverted Polymer Solar Cells with Directly Patterned Active Layer and Silver Back Grating," *J. Phys. Chem.,* vol. 116, no. 12, pp. 7200-7206, 2012.

[48] S. Kim, S. Na, J. Jo, D. Kim2 and Y. Nah., "Plasmon enhanced performance of organic solar cells using electrodeposited Ag nanoparticles," *Appl. Phys. Lett.,* vol. 93, p. 073307, 2008.

[49] S. Fischer, H. Steinkemper, P. Löper, M. Hermle, and J. C. Goldschmidt, "Modeling upconversion of erbium doped microcrystals based on experimentally determined Einstein coefficients," *J. Appl Phys.,* vol. 111, no. 1, p. 013109, 2012.

[50] S. Fischer, J. C. Goldschmidt, P. Löper, G. H. Bauer, R. Brüggemann, K. Krämer, D. Biner3, M. Hermle, and S. W. Glunz, "Enhancement of silicon solar cell efficiency by upconversion: Optical and electrical characterization," *J. Appl. Phys.,* vol. 108, no. 4, p. 044912, 2010.

[51] J. A. Briggs, J. A. Briggs, A. C. Atre, and J. A. Dionne, "Narrow-bandwidth solar upconversion: Case studies of existing systemsand generalized fundamental limits," *J. Appl. Phys. ,* vol. 113, no. 12, p. 124509, 2013.

[52] T. F. Schulze and T. W. Schmidt, "Photochemical upconversion: Present status and prospects for its application to solar energy conversion," *Energy Environ. Sci.,* vol. 8, no. 1, pp. 103-125, 2015.

[53] P. Gilbert, F. Auzel, J. Guillaume and K. Zahraman., "Below band gap IR response of substrate-free GaAs solar cells using two-photon upconversion," *J. Appl. Phys.,* vol. 351, pp. 4401-4402, 1996.

[54] A. Shalav, B. A. Richards and M. A. Green, "Luminescent layers for enhanced silicon solar cell performance:up-conversion," *SOLMAT,* vol. 91, no. 9, pp. 829-842, 2007.

[55] A. Pivrikas, G. Juska, AJ. Mozer, M. Scharber , K. Arlauskas, NS Sariciftci, H. Stubb and R. Osterbacka, "Bimolecular recombination coefficient as a sensitive testing parameter for low-mobility solar-cell materials," *Phys. Lett. Rev.,* vol. 94, p. 176806, 2005.

[56] L. J. A. Koster, V. D. Mihailetchi, and P. W. M. Blom, "Bimolecular recombination in polymer/fullerene bulk heterojunction solar cells," *Appl. Phys. Lett.,* vol. 88, no. 5, p. 052104, 2006.

[57] S. R. Cowan, W. L. Leong, N. Banerji, G. Dennler and A. J. Heeger, "Identifying a threshold impurity level for organic solar cells: enhanced first-order recombination via well-defined PC84BM traps in organic bulk heterojunction solar cells," *Adv. Funct. Mater.,* vol. 21, pp. 3083-3092, 2011.

[58] R. H. Page, K. I. Schaffers, P. A. Waide, J. B. Tassano, S. A. Payne, W. F. Krupke and W. F. Bischal, "Upconversion-pumped luminescence efficiency ofrare-earth-doped hosts sensitized with trivalent ytterbium," *J. Opt. Soc. Am. B,* vol. 15, no. 3, pp. 996-1007, 1998.

[59] M. F. G. Klein, G. Q. G. Medeiros, P. Kapetana, U. Lemmer and A. Colsmann, "Modeling approach to derive theanisotropic complex refractive indexof polymer:fullerene blends fororganic solar cells utilizingspectroscopic ellipsometry," *J. Photon Energy,* vol. 5, p. 057204, 2015.

[60] Y. Zhou, C. Fuentes-Hernandez, J. W. Shim, T. M. Khana and B. Kippelen, "High performance polymeric charge recombination layer for organic tandem solar cells," *Energy Environ. Sci.,* vol. 5, no. 12, pp. 9827-9832, 2012.

[61] J. Hou, H. Chen, S. Zhang, G. Li and Y. Yang, "Synthesis, Characterization, and Photovoltaic Properties of a Low Band Gap Polymer Based on Silole-Containing Polythiophenes and 2,1,3-Benzothiadiazole," *J. Am. Chem. Soc.,* vol. 130, no. 48, pp. 16144-16145, 2008.

[62] B. Yang, J. Cox, Y.Yuan, F. Guo, and J.Huang, "Increased efficiency of low band gap polymer solar cells at elevated temperature and its origins," *Appl. Phys. Lett.,* vol. 99, no. 13, p. 133302, 2011.

[63] A. Zusan, B. Gieseking, M. Zerson, V. Dyakonov, R. Magerle and C. Deibel, "The Effect of Diiodooctane on the Charge Carrier Generation in Organic Solar Cells Based on the Copolymer PBDTTT-C," *Scientific Reports,* vol. 5, p. Article Number: 8286, 2015.

[64] X. Ji, Z. Jiang, X. Chen, J. Zhou, L. Pan, F. Zhu, Z. Sun and S. Huang, "Highly efficient and air stable inverted polymer solar cells using LiF-modified ITO cathode and MoO3/AgAl alloy anode," *ACS Appl. Mater. Interfaces,* vol. 8, no. 6, pp. 3792-3799, 2016.

[65] R. Fan, L. Gu, X. Li, G. Fu and S, Yang, "High performance ternary organic solar cells using two miscible donor molecules based on PTB7-Th and DR3TBDTT," *Org. Electron.,* vol. 41, pp. 209-214, 2016.

[66] O. Madelung, Semiconductors: Data Handbook, Berlin: Springer-Verlag Berlin Heidelberg, 2012.

[67] W.B. Zhang, Q. Qu and K. Lai, "High-Mobility Transport Anisotropy in Few-Layer MoO3 and Its Origin," *ACS Appl. Mater. Interfaces,* vol. 9, no. 2, pp. 1702-1709, 2017.

[68] F. C. Krebs, Stability and Degradation of Organic and Polymer Solar Cells, West Sussex: John Wiley & Sons Ltd, 2012.